# Generation of functionally distinct T-cell populations by altering the viscoelasticity of their extracellular matrix

**Kwasi Adu-Berchie**[1,2], **Yutong Liu**[1,2], **David K.Y. Zhang**[1,2], **Benjamin R. Freedman**[1,2], **Joshua M. Brockman**[1,2], **Kyle H. Vining**[1,2,3,4], **Bryan A. Nerger**[1,2], **Andrea Garmilla**[5], **David J. Mooney**[1,2,*]

[1]John A. Paulson School of Engineering and Applied Sciences, Harvard University, Cambridge, Massachusetts, USA

[2]The Wyss Institute for Biologically Inspired Engineering Harvard University, Boston, Massachusetts, USA

[3]Dana-Farber Cancer Institute, Department of Medical Oncology, Boston, Massachusetts, USA

[4]Department of Preventative and Restorative Sciences, School of Dental Medicine, and Department of Materials Science and Engineering, School of Engineering and Applied Science, University of Pennsylvania, Philadelphia, PA, USA

[5]Harvard Medical School, Boston, Massachusetts, USA

## Abstract

The efficacy of adoptive T cell therapy is highly dependent on the generation of T cell populations that are able to both provide immediate effector function and long-term protective immunity. Inspired by the emerging consensus that T cell phenotype and function are inherently linked to their tissue localization, we present an approach to generate functionally distinct T cell populations via the physical properties of their surrounding matrix. A collagen type I based extracellular matrix (ECM) was engineered to allow for independent tuning of matrix stiffness and viscoelasticity, two features that characterize the mechanical properties of tissues. The mechanical properties of the ECM, particularly ECM viscoelasticity, regulated T cell phenotype and function, and the AP-1 pathway, which is a critical regulator of T cell fate. These observations were consistent with the profiles of T cells isolated from mechanically distinct tissues in cancer and fibrosis patients. The engineered ECM was then utilized to generate functionally distinct T cell populations from cells that received the same initial stimulation. Altogether these findings demonstrate the direct role of tissue viscoelasticity in directing T cell function and provide a strategy for generating functionally distinct T cell populations.

*Correspondence: David J. Mooney (mooneyd@seas.harvard.edu).
Underline indicates authors contributed equally

## Introduction

T cells play a critical role in the immune response to tumors and are characterized by their antigen specificity, and their long-term memory potential that establishes protective immunity[1–3]. Adoptive T cell therapy is an emerging area of immunotherapy where T cells are harvested from a patient, manipulated *ex vivo* and reinfused into the patient[4]. These T cells can either be tumor infiltrating lymphocytes (TILs), which are isolated from tumors, or more commonly autologous polyclonal T cells isolated from apheresed PBMCs[5]. Autologous T cells can be genetically modified into TCR T cells or Chimeric Antigen Receptor (CAR) T cells based on whether the antigen being recognized is in the presence or absence of MHC respectively[5]. While T cell therapy has shown remarkable promise, especially in hematological cancers, the efficacy of T cell therapies can be enhanced by generating T cell populations that provide both immediate and durable long-term protection against cancer[5–8].

The generation of CAR T cells and genetically modified TCR T cells involve *ex vivo* stimulation of isolated T cells prior to genetic manipulation[8,9]. Approaches to T cell stimulation have evolved from the labor-intensive use of purified autologous antigen presenting cells (APCs)[3,10] to more efficient artificial APCs presenting aCD3/aCD28 monoclonal antibodies, supplemented with growth factors such as IL-2 for T cell expansion[9,11]. Activated T cells are incubated with either viral vectors or non-viral transposon systems for stable CAR or TCR expression[12,13], or mRNA for more transient expression[14]. Most approaches aiming to generate various T cell populations *in vitro* are limited to altering the strength and duration of T cell stimulation[8,15]. Approaches that can further tune T cell phenotype for a given stimulation regimen could broaden the repertoire of T cells available for therapy.

Prior studies suggest that T cell phenotype is inherently linked to their location, and this is likely linked to the distinct properties of various anatomic locations[16–18]. In tissues, T cells encounter mechanical resistances in the form of stiffness and viscoelasticity as they engage extracellular matrices (ECM) like collagens, which are altered in pathologies like cancer and fibrosis. Stiffness describes a material's resistance to instantaneous deformation, whereas viscoelasticity, as exhibited by stress relaxation, is a distinct feature from stiffness that refers to a material's time-dependent mechanical response to applied strains[19,20]. The stress needed to maintain a particular deformation decreases more rapidly with time for minimally crosslinked, fast relaxing ECM (more viscous) than for more highly crosslinked, slow relaxing ECM (more elastic). Both tissue stiffness and viscoelasticity have been shown to independently influence the behavior of cells, including their proliferation, mobility and differentiation[20].

Here, we hypothesize that functionally distinct T cell populations can be generated by selectively tuning the mechanical properties of matrices in which cells are embedded, mimicking distinct mechanical properties of the tissue microenvironment. To address this hypothesis, a collagen type 1 based ECM model was first engineered to allow for independent tuning of matrix stiffness and viscoelasticity. Collagen type 1 was

utilized because it is a major ECM constituent in multiple tissues, forming the fibrillar structures that provide mechanical tissue integrity, as well as adhesion ligands for cell adhesion and migration[21]. To control for initial T cell activation, T cells received the same initial stimulation regimen before they were cultured in matrices with different viscoelasticity. In vivo, T cells are primed when antigen presenting cells sample, process, and present antigen to T cells on their major histocompatibility complex (MHC) proteins. However, the phenotype of these antigen presenting cells themselves could be influenced by their mechanical environment, complicating one's ability to determine how matrix mechanical properties regulate T cell activation. Consequently, we used synthetic CD3/CD28 dynabeads, which is the industry standard for CAR-T cell activation and expansion for clinical use, and which can be easily separated from T cells via the use of magnets before the cells are seeded in collagen matrices. T cell phenotype, in vitro cytotoxic function and cytokine secretion profiles, as well as in vivo function were analyzed, as was the AP-1 pathway, which has been shown to be a critical regulator of T cell activation, differentiation and exhaustion. The profiles of T cells cultured in the distinct mechanical environments was further compared to T cells derived from mechanically distinct tissues in cancer and fibrosis patients. Together, these studies further our understanding of the role of tissue mechanical properties in directing T cell function and provide a tool for generating functionally distinct populations of T cells.

## Results

### T cell phenotype varies in mechanically distinct tissues *in vivo*

First, to confirm and extend previous reports that aspects of the tissue microenvironment may regulate T cell phenotype in vivo, published scRNA-seq datasets were analyzed to compare CD8+ T cells located in tumors, adjacent normal tissues and blood for patients with non-small cell lung cancer (NSCLC)[22], liver cancer[23], and colorectal cancer[24], representing diverse mechanical environments. These analyses were performed for both pan T cells and T cells with shared TCR clonotypes between the tissue types. The three tissue types were selected because they span the spectrum between very soft, fast-relaxing (blood: a viscous fluid)[25] and stiff, slow-relaxing (tumor) [26,27] tissues. Umap plots of pan T cells showed distinct localization of T cells from the different tissue compartments, with increased overlap between T cells from tumors and those from their corresponding normal tissues compared to blood (Fig. 1a). Tumor T cell gene signatures were generated for each tumor type by performing differential gene expression analysis between tumor derived T cells and T cells in normal tissue and blood (Supplementary Table 2). These signatures were then applied to T cells from the different tissue compartments to compare their aggregate expression levels. T cells from the blood had the lowest expression of tumor T cell gene signatures, with T cells in adjacent normal tissue being intermediate (Fig. 1b). This trend was maintained when the same analysis was performed for T cells with shared TCR clonotypes (Fig. 1c). These results suggest that the tissue microenvironment may be playing a role in modulating T cell phenotype.

To better correlate the observed transcriptomic differences between T cells isolated from the different tissues with their microenvironment, and to further inform our choice of ECM

protein for subsequent studies, bulk sequencing from the TCGA dataset was analyzed to compare the relative expressions of canonical matrix proteins that are known to influence tissue mechanical properties. In particular, collagen type I (COL1A1) and lysyl oxidase (LOX), which is known to crosslink collagen fibers in vivo, were found to be differentially expressed in tumors relative to normal tissues for each tumor type (Fig. 1d).

## Synthesizing collagen-based ECM mimetic with tunable mechanical properties

We next engineered a collagen type I based ECM model to allow for independent tuning of matrix stiffness and viscoelasticity for T cell culture. Collagen type I was first modified with norbornene (Nb), which undergoes a highly selective bioorthogonal click reaction with tetrazine (Tz) moieties via inverse electron demand Diels-Alder[28]. Matrix stiffness was tuned by varying the collagen concentration, while the addition of local covalent crosslinking to the Nb-modified collagen post gelation with low molecular weight Tz crosslinkers regulated matrix viscoelastic properties without changing the stiffness (Extended figure 1a, Fig. 2a). Two collagen concentrations were utilized, as these yielded matrices which spanned the stiffness range of multiple soft tissues[29] (Extended Fig. 1b), as well as pre-malignant and malignant tumors[30–34]. Mechanical characterization of the matrices showed that while click crosslinking influenced matrix viscoelastic properties, as reflected in shear stress relaxation and loss angle of the matrices, it did not affect shear bulk stiffness values (Fig. 2b–c, Extended Fig. 1c). Further characterization by cryo-scanning electron microscopy (Cryo-SEM) and second harmonic generation imaging (SHG) showed that click crosslinking did not alter the fibrillar architecture or pore-size distribution of collagen matrices (Fig. 2d–e, Extended Fig. 1d), and did not affect collagen fiber length, waviness or angle between the fibers (Extended Fig. 1e–g). Importantly, analysis of local mechanical properties with nanoindentation confirmed similar storage moduli (G') for each collagen concentration but significantly different loss moduli (G") between fast and slow relaxing matrices (Extended Fig. 1h–i).

CD8+ T cells were subsequently isolated from healthy donors, activated, and subsequently cultured in fast relaxing (non-click crosslinked) or slow relaxing (click crosslinked), soft (2 mg/ml) or stiff (4 mg/ml) collagen matrices. After 3 days in the various matrices, the T cells showed notable phenotypic differences, driven more by changes in collagen viscoelasticity than by stiffness (Fig. 2f–h). In particular, flow cytometry analysis of CD8+ T cells showed higher expression of activation and inhibitory markers in slow relaxing matrices, while T cells in fast relaxing matrices exhibited higher memory marker expression, such as CD62L and CD45RA (Fig. 2f). These observations were consistent with multiple donors and across multiple independent experiments (Extended Fig. 2)

## Collagen modification and crosslinker have minimal effects on T cell adhesion and phenotype

Potential effects of collagen modification and the presence of methyltetrazine crosslinkers on T cell adhesion and phenotype were next investigated. T cells that were seeded on top of unmodified and Nb-modified collagen with and without methyltetrazine crosslinkers adhered similarly to their respective collagen matrices (Extended Fig. 3a). In addition, T cells remained highly viable in all matrix conditions (Extended Fig. 3b) and had

similar phenotypic profiles when they were embedded in unmodified collagen (Col) or in Nb-modified collagen (Col-Nb) (Extended Fig. 3c–e). The presence of methyltetrazine crosslinkers had some, but minimal effect on T cells cultured in unmodified collagen matrices (Col (+Linkers)), but had significant effects on T cells cultured in modified collagen (Col-Nb (+Linkers)), as expected due to changes in matrix viscoelasticity from the resultant crosslinking in the latter (Extended Fig. 3c–e). Importantly, PCA analyses confirmed our observations, with Col-Nb (+Linkers) being most different along PC1 (Extended Fig. 3f).

### ECM viscoelasticity modulates T cell phenotype in complex ECM

Even though collagen type I forms a significant fraction of many tissue ECMs, the effects of viscoelasticity within the context of a more complex ECM formulation was next studied. These studies were performed with an interpenetrating network (IPN) of Matrigel and collagen type I to mimic the complexity of tissue ECM. The viscoelasticity of the collagen-Matrigel IPN was again tuned by selectively and locally crosslinking collagen-Nb within the network with low molecular weight methyltetrazine crosslinkers. Bulk rheological characterization of the IPNs showed significant effects of click crosslinking on stress relaxation halftime and loss angle (Extended Fig. 4a). Importantly, similar to the observations made for the collagen-only matrices, alterations in viscoelastic properties led to significant changes in T cell phenotype (Extended Fig. 4b–e).

### Extracellular matrix viscoelasticity modulates T cell transcriptomic profile

To investigate how ECM viscoelasticity drives changes in the transcriptional landscape of T cells, scRNA-seq of CD8+ T cells cultured in fast relaxing and slow relaxing collagen matrices was next performed. Umap analysis showed distinct localization of the two T cell populations (Fig. 3a). Global differential expression identified upregulation of several conventional activation and inhibitory T cell markers, including *IL2RA* (CD25), *ENTPD1 (CD39)* (Fig. 3b), as well as *FAS, TNFRSF4 (OX40)* and *LAG3* (Extended Table 3) in slow-relaxing matrices compared to fast-relaxing matrices. In addition, transcription factors that have been implicated in T cell effector phenotype such as *PRDM1* (BLIMP-1) and *ZEB2* were also more highly expressed for T cells cultured in slow relaxing matrices. Of note, several genes related to the AP-1 pathway, including *JUN, ATF3, BATF* (Fig. 3b) and *FOS* and *FOSB*, in addition to some mitogen-activated protein kinases such as MAPK8, MAPK6 and MAPK1 (Extended Table 3) were enriched in T cells cultured in slow relaxing matrices. In contrast, T cells in fast relaxing matrices expressed higher levels of T cell memory markers and memory related transcription factors such as *CD62L, KLF2, CXCR3* and *S1PR4* (Fig. 3b, Extended Table 4).

We next performed consensus non-negative matrix factorization (cNMF)[35] to group genes into expression programs in an unsupervised manner, and investigate programs enriched for T cells in the different microenvironments. cNMF identified 15 gene expression programs, 4 of which were significantly enriched in T cells cultured in slow relaxing matrices and 2 in fast relaxing matrices (Fig. 3c–d). Module 5 was the most notably enriched module in slow relaxing matrices and included AP-1 pathway-related genes such as *JUN, ATF3, FOS, FOSB* and *JUNB* (Fig 3d, Extended Table 5). Unique genes from the 4 programs enriched

in slow relaxing matrices were combined into the Slow-Relaxing Module (SModule), and the 2 programs associated with fast relaxing matrices were grouped into the Fast-Relaxing Module (FModule). Umap overlay of aggregate expression levels of the SModule and FModule showed distinct localizations that mapped to regions of high T cell density in slow relaxing and fast relaxing matrices respectively (Fig. 3e). When the expression profiles of FModule and SModule were compared between plate-cultured T cells (i.e., 2D suspension culture with no collagen matrix), and T cells embedded in fast relaxing or slow relaxing collagen matrices, T cells in the slow relaxing collagen matrices were the most different, having the lowest expression of FModule and highest expression of SModule (Fig. 3f). Pathway enrichment analysis showed that the SModule was enriched for pathways related to TCR signaling, CD8+ T cell activation, and T cell cytotoxicity, indicating a more activated T cell state, while the FModule was enriched for genes related to leukocyte adhesion to endothelial cells (Fig. 3g).

Next, we applied the gene modules to a series of independently published RNA-seq datasets from both in vitro and in vivo studies to correlate our observed T cell states to independent studies involving T cell activation and tissue localization respectively. In a bulk RNA-seq dataset from activated and non-activated T cells in vitro[36], the SModule was significantly enriched in activated T cells while the FModule was enriched in the non-activated condition (Fig. 3h). The SModule was then applied to CD8+ T cells in tumors, adjacent normal tissue, and blood from the scRNA-seq datasets for NSCLC, liver cancer, colorectal cancer analyzed in Fig 1a–c, for both pan CD8+ T cells (Extended Fig. 5) or T cells with shared TCR clonotypes (Fig. 3i), in addition to a breast cancer dataset for pan CD8+ T cells (Extended Fig. 5)[37]. The trends for SModule expression were consistent with those in Fig. 1a–c, with T cells in tumors having the highest expression levels among the three tissue types, T cells in blood having the lowest, and T cells in normal tissue having intermediate expression levels.

## AP-1 Pathway is enhanced in T cells cultured in slow relaxing ECM in vitro, and in tumors and fibrotic tissues *in vivo*

Due to the observation that multiple AP-1 related genes were enriched in T cells from slow relaxing matrices, we performed AP-1 gene enrichment analysis on the cNMF modules. We saw significant enrichment of the AP-1 pathway in cNMF Module 5 (Extended Fig. 6a), which was the most notable module in slow relaxing matrices. Consequently, we hypothesized that ECM viscoelasticity modulates the AP-1 pathway, which in turn drives the observed T cell phenotypic profiles. To test the relevance of this hypothesis in vivo, we investigated the expression levels of cNMF Module 5 (AP-1 Module) in T cells derived from tumors, adjacent normal tissue, and blood from scRNA-seq datasets for NSCLC, liver cancer, colorectal cancer for T cells with shared TCR clonotypes (Extended Fig. 6b). We observed the highest expression levels in tumors, while T cells in blood had the lowest expression levels of the AP-1 Module. T cells in adjacent normal tissues had AP-1 expression levels that were again intermediate.

To examine whether the observations of AP-1 enrichment in T cells are specific to cancer, or more broadly to conditions with altered matrix mechanics, a similar analysis was performed in the context of fibrosis. Fibrosis is generally accompanied by increased ECM

deposition and crosslinking[38], resulting in changes in matrix stiffness and viscoelasticity. We investigated the AP-1 pathway in T cells located in fibrotic tissues by first generating cNMF modules from CD8+ T cell data derived from a published liver cirrhosis scRNA-seq dataset[39] and two IPF datasets[40,41], which compared fibrotic tissues to adjacent normal tissues. These cNMF modules were generated from the published datasets themselves and were independent of the modules generated in this study in vitro. We then performed AP-1 gene enrichment analyses and saw AP-1 enriched modules in all the fibrosis datasets investigated (Extended Fig. 6c–d). Importantly, the expression levels of the AP-1 modules were significantly higher in fibrotic tissues than in normal tissues. This trend was maintained when we investigated the expression levels of the in vitro generated AP-1 module in the fibrotic tissues (Extended Fig. 6e).

The phosphorylation states of a number of transcription factors and kinases related to the AP-1 pathway were next examined to further probe AP-1 transcriptional regulation after T cells are cultured in collagen matrices of varying stiffness and viscoelasticity (Extended Fig. 7a). For all transcription factors investigated, there was increased phosphorylation in T cells cultured in slow relaxing matrices for both CD4+ and CD8+ T cells. Principal component analysis (PCA) revealed that ECM viscoelasticity was the main driver of the differential phosphorylation states (Extended Fig. 7b). In addition to c-Jun and p-c-Jun, PCA loadings identified features such as pPyk2, pPlcg1, pPlcg2, pMAPK8, pMAPK14 and pCD3z as important factors underlying the observed PCA trend (Extended Fig. 7c).

## Matrix viscoelasticity impacts pattern of AP-1 protein expression

We next examined the patterns of AP-1 protein expression and their interactions, specifically with c-Jun, due to their importance in the regulation of T cell phenotype and function[42]. In particular, c-Jun and c-Fos are canonical AP-1 partners that have been shown to enhance IL2 production[42]. BATF promotes effector T cell differentiation but also drives exhaustion[43–45]. JunB has been shown to enhance Th17 differentiation and IL2 production, but also promotes T cell exhaustion and effector Treg differentiation[46–49]. Flow cytometry analyses after culturing T cells in fast and slow relaxing matrices showed that T cells cultured in slow relaxing matrices had enhanced expression of c-Jun, c-Fos, and BATF (Fig. 4a–b). Additionally, T cells from slow relaxing matrices exhibited higher interaction of c-Fos, JunB and BATF with c-Jun, as analyzed by c-Jun co-immunoprecipitation of cell lysates to assess AP-1 binding partners (Fig. 4c).

The ability of c-Jun to mediate effects of viscoelasticity on T cell phenotype was directly tested by blocking c-Jun function with the SP600125 Jun N-terminal kinase inhibitor[50]. Umap and K-means analyses of T cell phenotypes showed that SP600125 abrogated the effects of matrix viscoelasticity (Fig. 4d) and led to increased expression of memory markers in all conditions (Fig. 4e). PCA analysis confirmed these results. The slow relaxing matrix without SP600125, and all conditions with SP600125 were located at the two extremes of PC1, while plate culture and fast relaxing matrix conditions without SP600125 were intermediate (Fig. 4f). Together, these findings demonstrate that the patterns of AP-1 protein expression and their interactions with c-Jun can be modulated by ECM viscoelasticity.

## ECM viscoelasticity does not select for specific T cell clones

To assess whether the observed phenotypic differences imparted by matrix viscoelasticity are due to the selection and persistence of specific T cell clones, we performed single cell RNA-sequencing with TCR sequencing using T cells from a different donor. Umap analysis on pan T cells from the different conditions showed distinct localization of T cells from plate-culture, fast relaxing and slow relaxing matrix conditions (Fig. 5a). The Slow-Relaxing Module (SModule), generated from the previous scRNA-seq in Fig. 3, was applied to pan T cells from this dataset to investigate consistency across different donors. The trends for SModule expression were consistent with those in Fig. 3, with T cells cultured in slow relaxing matrices having the highest expression of SModule (Fig. 5b).

To explore the potential of ECM viscoelasticity in skewing the TCR, the profile of T cell receptor β (TRβ), a component of the TCR heterodimer, was investigated. Similar frequency distributions were observed for the different TRβV genes as a function of ECM condition (Extended Fig. 8a). In addition, a Venn diagram of the TRβV genes showed that 96% of the genes were present in all the conditions (Extended Fig. 8b). Shannon entropy, which estimates the diversity within a specific population, showed similar TRβV diversity between T cells cultured in fast relaxing matrices, slow relaxing matrices, and plate-culture, as well as their parent T cell population (Pre-Gel) (Extended Fig. 8c). Importantly, when the SModule was applied to the T cells grouped by TRβV gene, the slow relaxing matrices had the highest expression across all TRβV genes (Extended Fig. 8d).

We next investigated the effects of ECM viscoelasticity on CDR3 profiles and the persistence of T cell clonotypes. First, it was observed that TCRβ CDR3 length distribution was similar across all the conditions, including in the parent T cell population (Fig. 5c). Assessment of TCR clones revealed that all the conditions had similar clonotypic diversity as estimated by Shannon entropy (Fig. 5d). The T cells generally had unique clonotypes, with only 3.7% of T cells being clonal (clones observed in >1 cell) (Fig. 5e). Dominant clones (clones observed in >3 cells) were not limited to specific conditions, but were shared across multiple conditions, with 5 clones being shared among all conditions (Fig. 5f). Importantly, T cells with shared TCRs derived from the various matrix conditions were transcriptomically different, with the T cells cultured in slow relaxing matrices having the highest expression of the SModule (Fig. 5g). We also hypothesized that if the matrix is acting by selecting specific T cell clones, whose phenotypes persist over time, then there should be a correlation between the transcriptomic profiles of those T cell clones before and after matrix culture. However, correlation analysis between individual T cell clones before and after their culture in collagen matrices showed weak correlation for the fast relaxing matrix condition (Pearson correlation=0.38) and no correlation for the slow relaxing matrix condition (Pearson correlation=−0.089) (Fig. 5h–i). Together, these findings suggest that ECM viscoelasticity directly modulates T cell phenotype, and does not select specific T cell clones which persist over time.

## ECM viscoelasticity imprints long-term T cell phenotype

To investigate the extent to which the differences in T cell phenotypes persist after being exposed to matrices with different viscoelasticity, T cells were first embedded in either fast

or slow relaxing collagen matrices for 3 days, after which they were cultured in suspension for 4 days. The T cells expanded and remained viable post matrix culture (Extended Fig. 9a). Umap, K-means and PCA analyses showed that T cell phenotypes remained distinct after 4 days of suspension culture, with T cells harvested from slow-relaxing matrices being enriched in clusters with higher expression of activation markers: clusters 4, 5, 6, 8 (Extended Fig. 9b–c). Importantly, this trend was maintained when the T cells harvested from the various matrix conditions were re-stimulated with dynabeads in suspension (Extended Fig. 9f–j).

To further explore the role of ECM viscoelasticity on imprinting long-term T cell phenotype, T cells were serially passaged as follows: from fast relaxing to fast relaxing matrices (Fast-Fast), from fast relaxing to slow relaxing matrices (Fast-Slow), from slow relaxing to fast relaxing matrices (Slow-Fast) and from slow relaxing to slow relaxing matrices (Slow-Slow) (Fig. 6a). Flow cytometry analyses revealed an impact of the prior matrix condition on the phenotype of the T cells in the latter matrix. In particular, Umap, K-means and PCA analyses showed that T cells from Fast-Fast and Slow-Slow conditions were the most different, with the Fast-Slow and Slow-Fast conditions being intermediate (Fig. 6b–e). Importantly, when the Euclidean distances between a) Fast-Fast and Fast-Slow and b) Slow-Slow and Slow-Fast conditions were compared, it was found that there was a greater distance between Fast-Fast and Fast-Slow (more dissimilar) than Slow-Slow and Slow-Fast conditions, suggesting that slow relaxing matrices had a greater impact on modulating T cells that have been previously cultured in fast relaxing matrices than vice versa (Fig. 6f).

We next profiled T cells after embedding them in collagen matrices for different timepoints (3 days and 7 days), and subsequently culturing the cells in suspension to investigate if the effects of ECM viscoelasticity on imprinting T cell phenotype is time dependent. Consistent with previous observations, T cell phenotype was modulated by ECM viscoelasticity at both harvest timepoints (Extended Fig. 10a–e). When T cells were harvested from collagen matrices on days 3 and 7, and subsequently cultured in suspension for 7 additional days, they maintained the T cell phenotype imprinted by the specific matrix mechanical properties in a manner dependent on the duration of initial gel culture (Extended Fig. 10f).

### ECM viscoelasticity modulates the phenotypes of T cells subjected to different modes of prior activation

To understand the generalizability of ECM viscoelasticity in modulating T cell phenotypes in relation to mode of prior activation, T cells were either activated with CD3/CD28 or CD3/CD28/CD137 dynabeads, before embedding in collagen matrices, with the latter known to enhance memory T cell enrichment[51]. Consistent with previous data, flow cytometry analyses showed an impact of ECM viscoelasticity in modulating T cell phenotype after CD3/CD28 activation. Umap, K-means, and PCA analyses confirmed these differences, with T cells harvested from slow-relaxing matrices being enriched in clusters with higher expression of activation markers: Clusters 1, 4, 8 (Extended Fig. 11a–d). Importantly, these phenotypic differences were maintained when the T cells were activated with CD3/CD28/CD137 dynabeads prior to matrix culture (Extended Fig. 11e–h).

## Tuning matrix viscoelasticity leads to functionally distinct T cells.

We next investigated whether T cell populations that are functionally distinct resulted from culture in the engineered matrices with distinct levels of viscoelasticity, and how these populations would evolve when the strength of stimulation are altered. First, anti-CD19 CAR T cells were cultured in ECM with varying stiffness and viscoelasticity after exposure to different strengths of antigenic stimulation, phenotypically profiled and functionally tested for their cytotoxic potential and effector cytokine production upon co-culture with Raji tumor cells. Umap analyses of T cell phenotypes showed distinct localization of T cells cultured in fast relaxing and slow relaxing collagen matrices for all the activation regimes tested (Fig. 7a, Extended Fig. 12a–b). T cells in slow relaxing matrices expressed higher levels of activation and inhibitory markers and lower levels of memory markers (Fig. 7b, c). Functionally, anti-CD19 CAR T cells cultured in slow relaxing matrices showed higher killing of Raji tumor cells in vitro, with these differences being more substantial as the level of acute stimulation was increased (Fig. 7d). Increased killing capacity was accompanied by higher expression of a number of effector molecules, including IL2, Granzyme B, and TNF-α (Fig. 7e). The increased cytotoxicity observed for T cells cultured in slow relaxing matrices was highly positively correlated with the expression of c-Jun, c-Fos and BATF (Extended Fig. 12c). Similar results were obtained when the in vitro cytotoxicity experiment was repeated with a different donor, including a plate-cultured T cell condition (i.e., no collagen matrix condition). Umap, K-means, and PCA analyses of T cell cytokine profiles after co-culture of anti-CD19 CAR T cells with Raji tumor cells showed differential cytokine profiles dependent on the matrix condition (Extended Fig 13a–e). This corresponded to differences in T cell cytotoxicity, with T cells cultured in slow-relaxing matrices showing the highest killing compared with plate-cultured T cells and T cells cultured in fast-relaxing matrices (Extended Fig. 13f).

We next explored T cell functionality as a function of viscoelasticity for TCR T cells using a different tumor type and in a different species to understand the generalizability of these observations. We first cultured mouse Pmel-1 T cells, which recognize the gp100 epitope on B16-F10 melanoma cells[52,53], in collagen matrices of different viscoelasticity, and subsequently co-cultured these T cells with B16-F10 tumor cells. Pmel-1 T cells cultured in slow relaxing matrices had the best killing relative to plate-culture and fast relaxing matrix conditions (Extended Fig. 13g).

To investigate if the in vitro functional differences corresponded to in vivo therapeutic outcomes, anti-CD19 CAR T cells cultured in fast and slow relaxing matrices were adoptively transferred into tumor-bearing mice in a luciferized Raji xenograft lymphoma model. IVIS imaging of Raji tumor burden and mouse survival showed consistency between in vitro and in vivo observations. NSG mice treated with anti-CD19 CAR T cells first cultured in slow relaxing matrices had lower tumor burden and significantly better survival than mice treated with the same number of T cells from fast relaxing matrices (Fig. 7f–h).

### ECM viscoelasticity modulates the phenotype and function of T cells undergoing chronic stimulation

We sought to assess the effects of ECM viscoelasticity on T cells undergoing chronic stimulation in the matrices, specifically investigating their AP-1 protein expression and interactions, as well as their phenotype and function. To achieve chronic stimulation within the matrices, we utilized Transact, 50 nm polymeric nanoparticles conjugated with aCD3/aCD28[54], as their small size is expected to minimally impact the bulk mechanics of the gel, and enable them to freely diffuse within the micron-scale pores of the gels. AP-1 protein analysis of T cells chronically stimulated in slow relaxing matrices maintained higher expression of c-Jun (Extended Fig. 14a–b), BATF, and JunB but expressed lower levels of c-Fos compared with cells in corresponding fast relaxing matrices (Extended Fig. 14b). c-Jun co-immunoprecipitation of cell lysates showed that T cells that received chronic stimulation in slow relaxing matrices had higher binding of JunB and BATF but not c-Fos (Extended Fig. 14c). Importantly, the amount of JunB and BATF bound to c-Jun increased markedly when the T cells were cultured in slow relaxing matrices with chronic stimulation, as compared to T cells in fast relaxing matrices (Extended Fig. 14c). In terms of the changes in the individual AP-1 proteins between acute and chronic stimulation, larger increases in BATF and JunB expression were found for slow relaxing matrices after chronic stimulation, while c-Fos, FosB, and c-Jun increased more with fast relaxing matrices (Extended Fig. 14d).

Finally, anti-CD19 CAR T cells were cultured in matrices with chronic stimulation, phenotypically profiled and tested for their cytotoxic potential and effector cytokine production. Phenotypic analyses revealed that T cells in slow relaxing matrices showed higher expression of activation and inhibitory markers and lower memory marker expression (Extended Fig. 14e–f). In contrast to T cells without chronic stimulation, the T cells from slow relaxing matrices exhibited poorer killing capacity than those in fast relaxing matrices after chronic stimulation (Extended Fig. 14g). This inverse killing trend corresponded to impaired IL2 and lower Granzyme B production in T cells cultured in slow relaxing matrices, even though they generally maintained higher levels of IFN-γ and TNF-α (Extended Fig. 14h). c-Jun, BATF and JunB expression were found to be negatively correlated with cytotoxic potential when the T cells received chronic stimulation in the matrices (Extended Fig. 14i), while c-Fos remained positively correlated with T cell cytotoxic potential.

## Discussion

A collagen type I based ECM model was engineered that allows for independent tuning of matrix stiffness and viscoelasticity, and used to demonstrate that the mechanical properties of tissues regulate T cell phenotype, with viscoelasticity as the dominant driver of these phenotypic differences. These observations are consistent with T cell profiles obtained from mechanically distinct tissues in cancer and fibrosis patients, and are highlighted by an enrichment in the AP-1 pathway. Importantly, functionally distinct T cell populations were generated from a population of cells that received the same prior stimulation by tuning ECM viscoelasticity.

An in vitro collagen based system was developed in which viscoelasticity can be varied independently of the initial elastic modulus by utilizing a combination of non-covalent and permanent covalent bonds. Adding covalent bonds only to regions of the network that are already in close spatial contact (e.g., already crosslinked physically) leads to minimal changes in the moduli, but dramatic alterations in the viscoelastic properties (e.g., rate of stress relaxation). Importantly, a sequential crosslinking approach was used here, in which physical gelation occurs first, followed by local covalent crosslinking using small biorthogonal crosslinking molecules. This approach preserves a consistent collagen architecture and pore size distribution. While other studies have reported an impact of substrate stiffness on TCR interactions utilizing 2D surfaces or coated particles[55–63], or on T cell activation using hydrogels with large pores that effectively create a flat/curved culture surface[64], or only varying collagen density[65], this is the first strategy aimed at generating functionally distinct T cell populations by tuning tissue-level viscoelasticity. This collagen system is the first to report a crosslinking mechanism that successfully decouples ECM stiffness from viscoelasticity, and the crosslinkers themselves had minimal impact on the phenotype of T cells. Further mechanical characterization and analyses could provide valuable additional insights into the viscoelastic behavior of these matrices. Developing frameworks across the field for mechanical testing of different substrates could serve as guidelines for the future design and iterations of these matrices. Modifying collagen with other click groups could expand the utility of this matrix system in the future. By demonstrating that more complex ECM can be developed by generating IPNs of collagen-Nb and other ECM proteins of interest, this system can also be used to study the impact of more complex cell-matrix interactions.

We demonstrate a direct link between ECM mechanics and T cell phenotype in vitro that it is consistent with clinical data, and is highlighted by an enrichment in the AP-1 pathway. In vitro, T cells cultured in slow relaxing collagen matrices were found to have higher expression of activation and inhibitory markers, while T cells cultured in fast relaxing matrices have higher expression of memory markers. Plate cultured T cells also showed distinct phenotypes with lower expression of activation and inhibitory markers relative to T cells cultured in slow relaxing matrices. It is important to note that plate-culture provides a mechanically diverse environment to cells. Cells engaged with the surface encounter a highly inelastic surface while those in suspension are surrounded by a viscous cell culture medium. It could be helpful for future studies to decouple the net mechanical effects of the viscous media from the inelastic surface of the plate. *In vivo*, T cells in mechanically distinct tissue compartments are phenotypically different, as demonstrated by the transcriptomic profiles of both pan CD8+ T cells and T cells with shared TCR clonotypes isolated from the blood, adjacent normal tissues and tumors of multiple tumor types. These findings are consistent with the growing acceptance that the location of T cells can be important for their phenotype, as seen in memory subtypes such as tissue resident memory T cells, which are important for the recall response to antigen[17,66,67]. A strikingly conserved trend was observed when T cells from blood, adjacent normal tissues, and tumors were internally compared, and when the in vitro-derived cNMF gene signature for T cells cultured in slow relaxing matrices was examined in these cells. The AP-1 pathway was found to be highly modulated by ECM viscoelasticity in vitro and showed a consistent trend between

mechanically distinct tissues in multiple tumor and fibrotic studies *in vivo*. Recent studies have shown that the AP-1 pathway, specifically the activation of c-Jun in fibroblasts, is a hallmark feature and possibly a unifying mechanism for multiple fibrotic diseases[68–70]. While our study took an agnostic approach to investigate the effects of ECM stiffness and viscoelasticity on T cells, the convergence of the data on AP-1 is indicative of the central role it plays in the cellular response to ECM mechanics. Our findings also suggest that therapies targeting the ECM viscoelasticity may directly impact T cell biology and fate.

TCR analyses from the different matrix conditions suggested that ECM viscoelasticity directly modulates T cell phenotype and does not select for specific clones that persist over time. The weak correlation observed between T cell phenotypes before and after their culture in fast relaxing matrices, with no correlation observed in slow relaxing matrices, suggests that slow relaxing matrices have a stronger effect on T cell phenotype than fast relaxing matrices. This is supported by the serial culture experiment, where T cells from fast relaxing matrices that were subsequently embedded in slow relaxing matrices were more impacted than T cells from slow relaxing matrices that were then embedded in fast relaxing matrices.

By tuning ECM viscoelasticity, functionally distinct T cell populations were generated, which have different patterns of AP-1 protein expression and interactions. In vitro findings suggest that slower relaxing ECM generate T cells that offer rapid response to antigen, while faster relaxing ECM may generate a slower cytotoxic response. These observations were consistent with the in vivo xenograft lymphoma model, where mice treated with T cells from slow relaxing matrices showed better therapeutic responses. Multiple studies have established that the AP-1 pathway is integral to T cell activation, effector differentiation, anergy and exhaustion[43–45,47–49,71,72]. Further, the relative expression of the different AP-1 proteins, and their interactions, are key to their ultimate function in T cells, and T cell exhaustion can be driven by an imbalance between activating and regulatory AP-1 complexes[42]. Our studies similarly find that distinct patterns of AP-1 protein expression and interactions result in T cell populations within matrices of distinct viscoelasticity, in a manner dependent on the length of stimulation.

The findings from this study support in vivo reports that tissue localization is essential to T cell fate, and identify tissue viscoelasticity as an important mechanical parameter that could be regulating T cell phenotype and function. Based on the principle, we demonstrate a strategy to generating functionally distinct T cell populations by tuning ECM viscoelasticity. Beyond the matrix platform presented and disease implications of our findings, this study motivates the exploration of T cell manufacturing approaches that incorporate viscoelasticity as a parameter in generating the desired T cell products for specific therapeutic applications.

## Extended Data
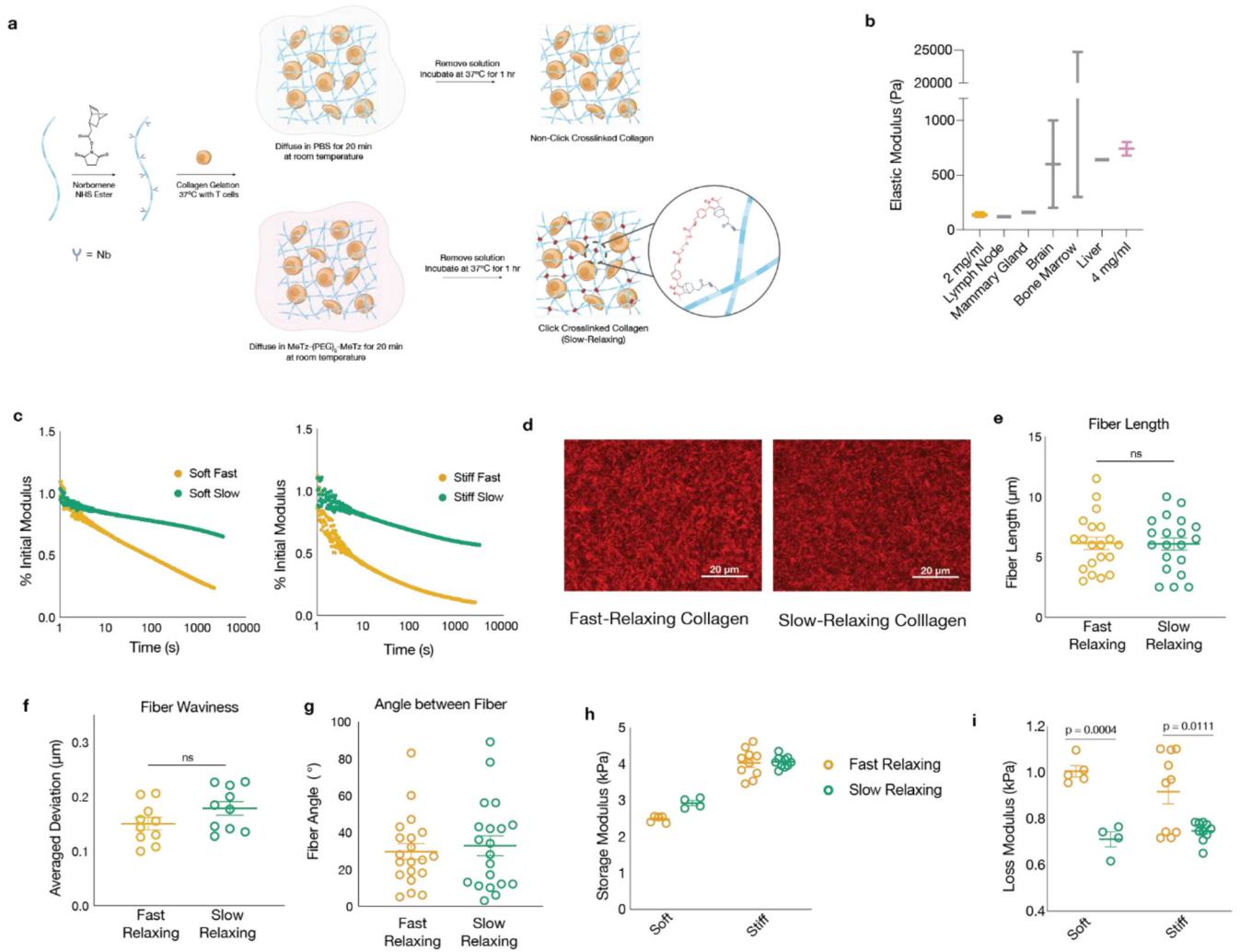


**Extended Fig. 1. Material synthesis and characterization.**

a. Collagen is modified with norbornene using NHS and gelled at 37°C with T cells. A low MW divalent crosslinker containing two methyltetrazines is diffused into gels at room temperature until equilibrated with the surrounding solution, to achieve even distribution within the gel. Subsequently increasing the temperature allows covalent crosslinks to form between norbornene and methyltetrazine functionalities. b. Comparison of Young's moduli for soft and stiff gels to those of published different soft tissues. c. Stress relaxation profiles of fast relaxing and slow relaxing, soft (left) and stiff (right) collagen matrices. d. SHG images for 2mg/ml fast relaxing and slow relaxing collagen gels. e-g. Quantification of fiber length (e), waviness (f) and angle between fibers (g) for fast and slow relaxing matrices. P-values were determined by performing two-tailed unpaired t-test. h-i. Storage and loss moduli determined using nanoindentation on collagen matrices. P-values were determined by performing two-tailed unpaired t-test for n=4 to n=10 indents.
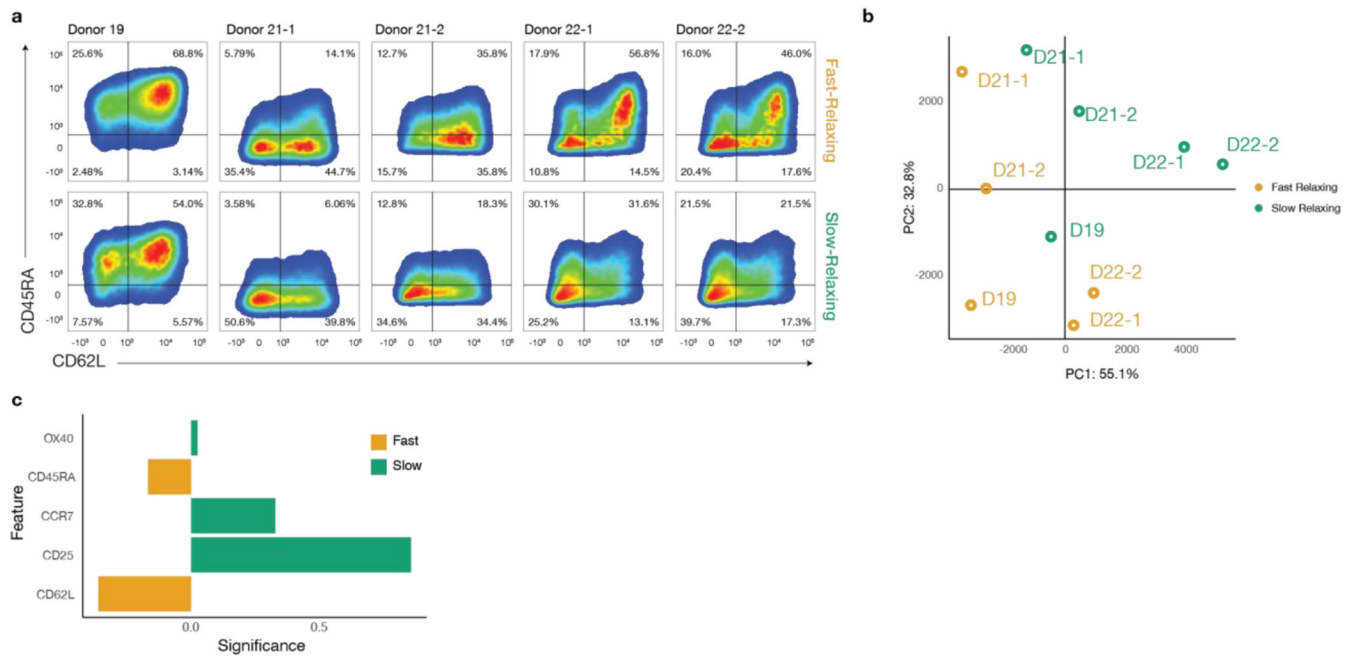
**Extended Fig. 2. ECM modulation of T cell phenotype using multiple donors and across independent experiments.**

a. Representative flow cytometry plots showing CD62L and CD45RA expression for T cells cultured in soft fast and soft slow relaxing gels after 4 days of activation for multiple donors and across multiple independent studies. For donors used for independent studies, the study number is indicated after the donor number. b. PCA plot showing that ECM viscoelasticity drives phenotypic differences along both principal components 1 and 2. c. PCA loadings for PC1 showing relative importance of input features. Data shows pooled samples n=2-3 for 3 donors across 5 independent experiments.
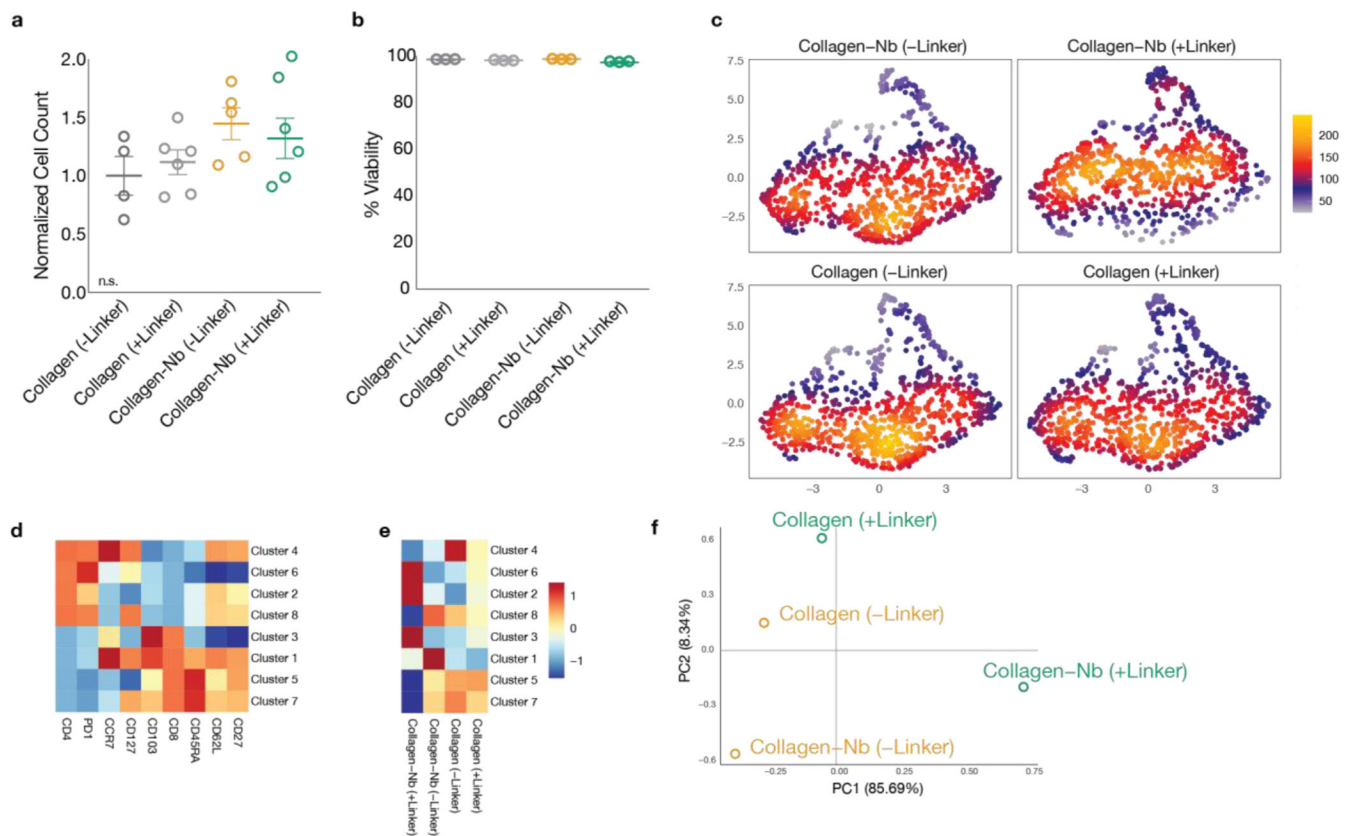
**Extended Fig. 3. Collagen modification and crosslinker have minimal effects on T cell adhesion and phenotype.**

a. Adhesion of T cells seeded on top of unmodified collagen or norbornene modified collagen (Collagen-Nb) with or without methyltetrazine linkers (n=4-6 replicates). b. Viability of T cells embedded in collagen matrices with or without norbornene modification and crosslinker. c. Umap plots of T cells phenotyped by flow cytometry after embedding in collagen matrices with or without norbornene modification and crosslinker. d-e. K-means clustering was performed on pooled T cells from all experimental conditions. d. Heatmap plot showing characteristic markers for each cluster. e. Heatmap plot showing the frequencies of cells per condition for each cluster. f. PCA plot showing relative similarities between the different conditions. Data for c-f show pooled samples for n=3 replicates.
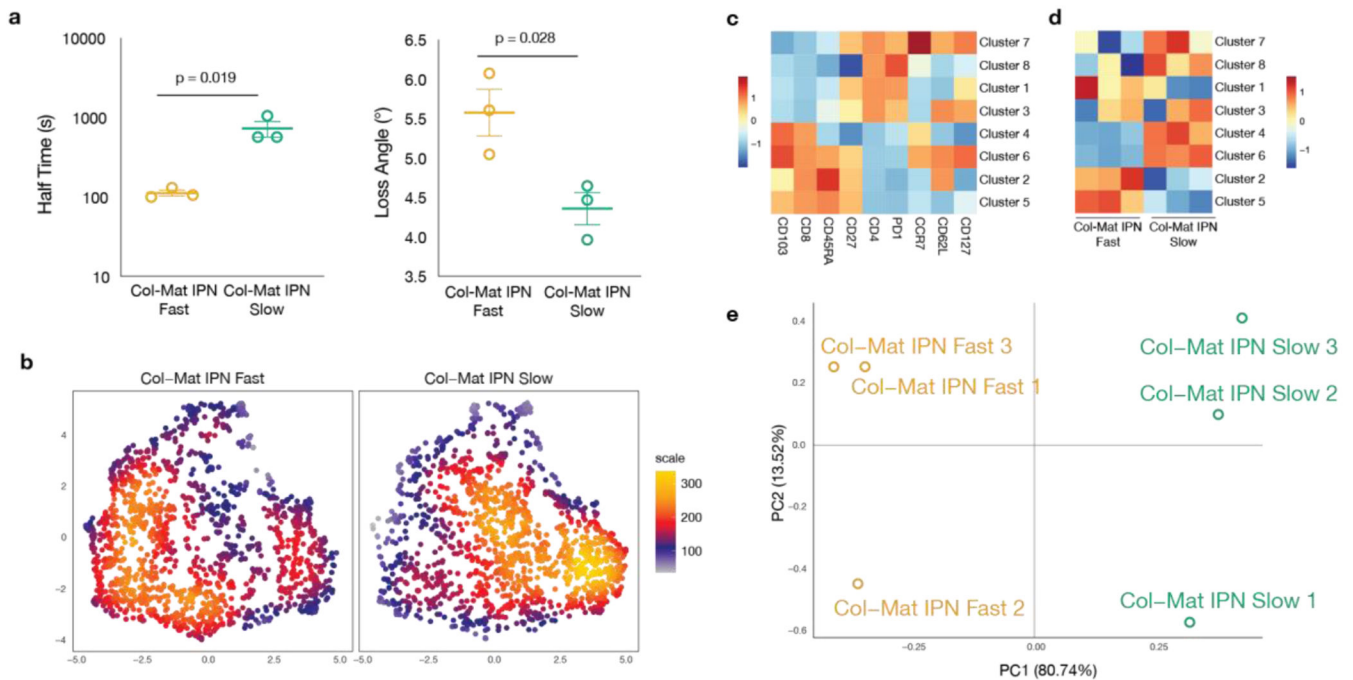
**Extended Fig. 4. ECM viscoelasticity modulates T cell phenotype in complex ECM.**
a. Stress relaxation half time (left) and loss angle (right) measurements of fast relaxing and slow relaxing collagen-matrigel IPNs (Col-Mat IPN). P-values were determined by performing two-tailed unpaired t-test for n=3 replicates. b. Umap plots of phenotyped T cells after embedding in fast and slow relaxing Col-Mat IPNs. Data for b shows pooled samples for n=3 replicates. c-d. K-means clustering was performed on pooled T cells from all experimental conditions. c. Heatmap plot showing characteristic markers for each cluster. d. Heatmap plot showing the frequencies of cells per condition for each cluster. e. PCA plot showing relative similarities between the different conditions.
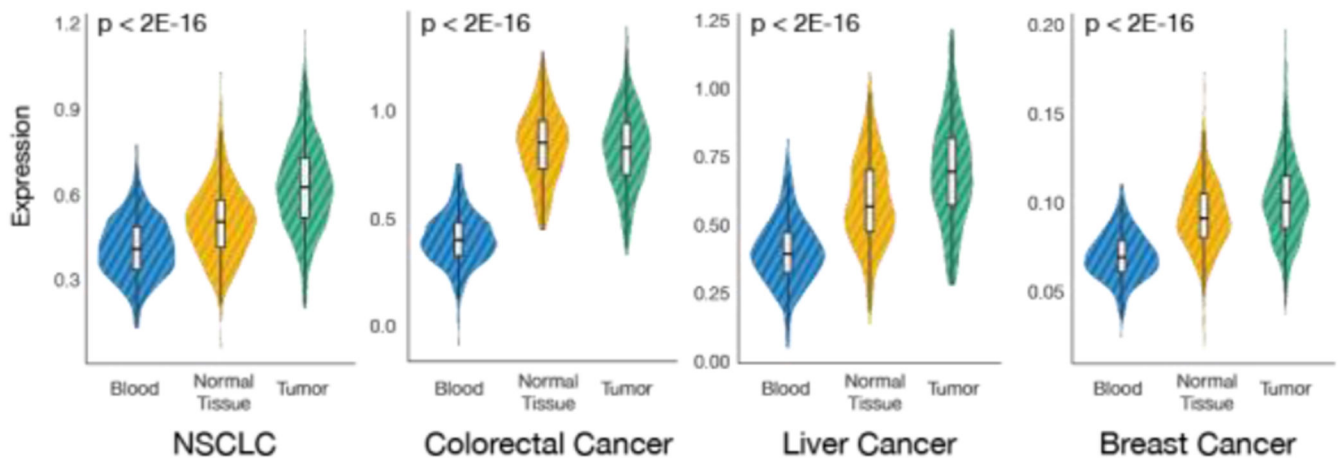


**Extended Fig. 5. Application of in vitro generated modules to pan T cells in tumor patients.**

Violin plots comparing expression levels of SModule for pan CD8+ T cells tumors, adjacent normal tissues and blood for NSCLC, liver cancer and colorectal cancer. P-values were determined by using two-tailed one-way Anova.
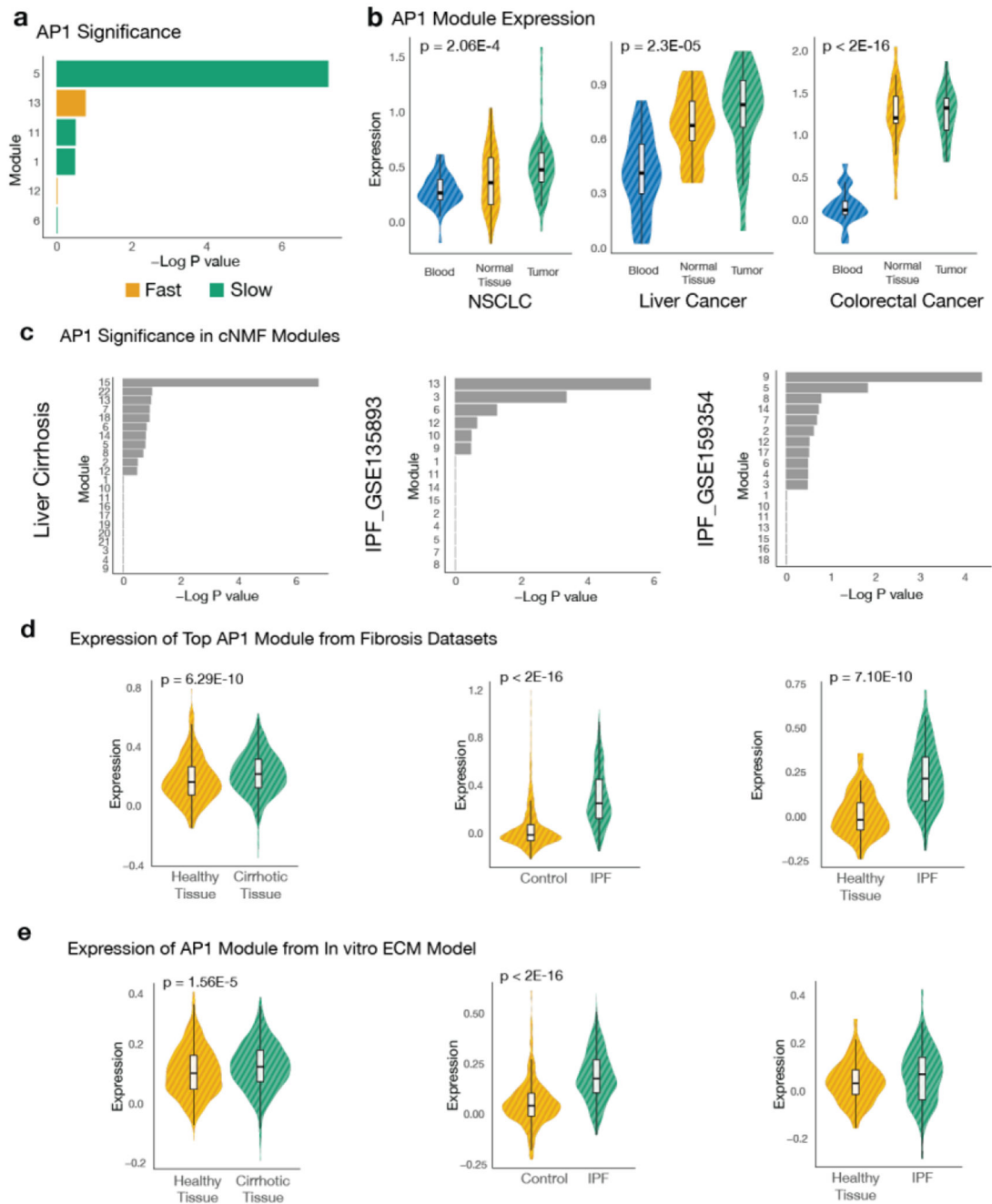


**Extended Fig. 6. AP-1 pathway is modulated by matrix mechanics.**
a-b. AP-1 pathway analysis was performed on enriched cNMF modules from Fig 3. a. Relative significance of AP-1 related genes in cNMF modules, showing significant AP-1 enrichment in Module 5. b. Violin plots comparing expression levels of Module 5 (AP-1

Module) for T cells with shared TCR clonotypes in tumors, adjacent normal tissues and blood for NSCLC, liver cancer and colorectal cancer. P-values were determined by performing two-tailed one-way Anova. c-d. AP-1 pathway analysis was performed on cNMF modules generated from the indicated fibrosis datasets. c. Relative significance of AP-1 related genes in cNMF modules. d. Violin plots comparing the expression levels of the top AP-1 module in CD8+ T cells derived from healthy and fibrotic tissues for each fibrosis study. e. Violin plots comparing expression levels of our *in vitro* generated AP-1 Module in CD8+ T cells derived from healthy and fibrotic tissues for the same datasets. P-values were determined by using the Wilcoxon Rank Sum test.
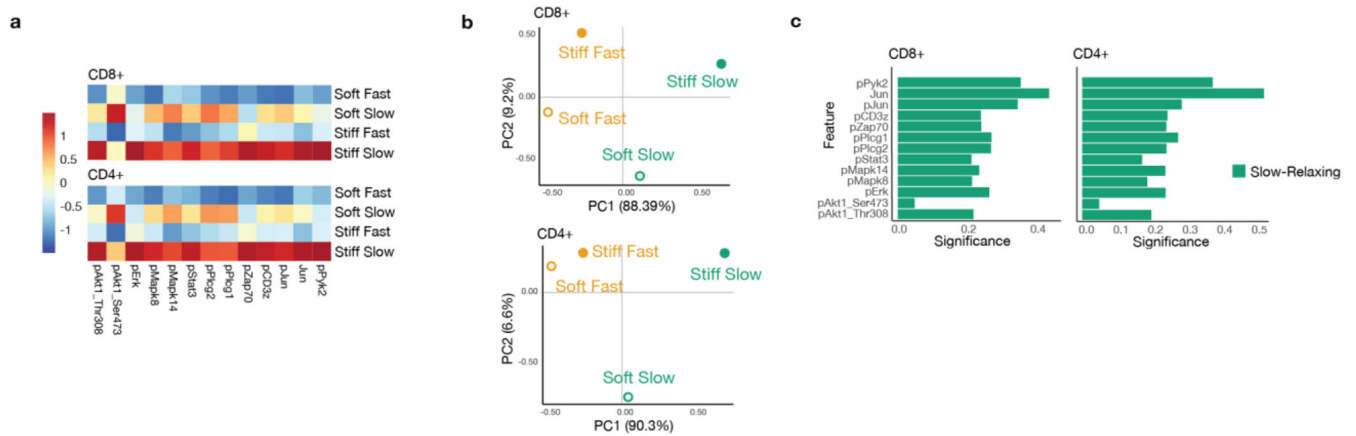


**Extended Fig. 7. Phosphorylation states of transcription factors and kinases known to impact or be impacted by AP-1.**

a. Heatmap plots comparing expression and phosphorylation levels of different transcription factors and kinases for the different gel conditions. b. PCA plots comparing the relative similarities between the different collagen conditions. c. PCA loadings for PC1 showing the relative significance of features that drive the observations in b. Data shows pooled samples for n=3.
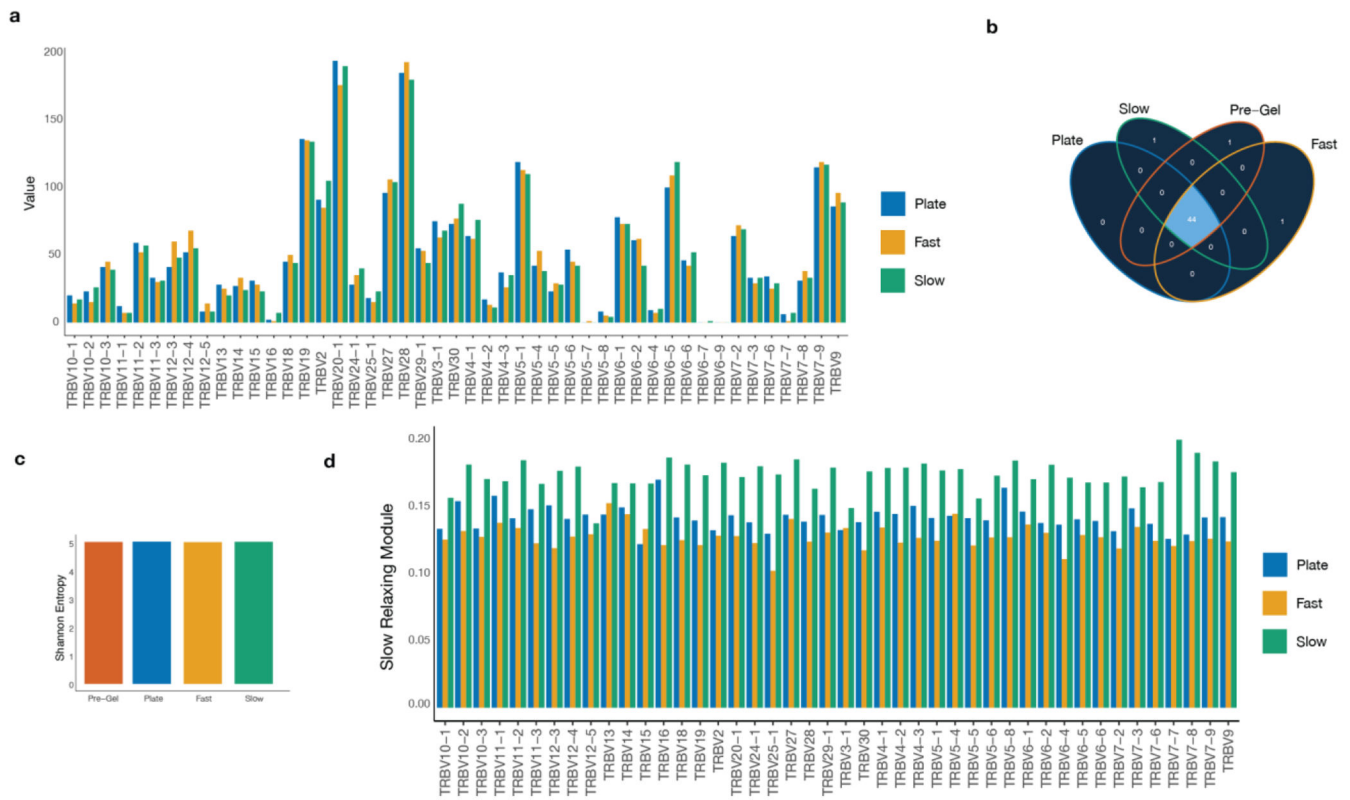
**Extended Fig. 8. T cell receptor β (TRβ) profile is not skewed by ECM viscoelasticity.**
a. Frequency distribution of the different TRβV genes for plate-cultured T cells, T cells embedded in fast-relaxing and slow relaxing matrices. b. Venn diagram showing the distribution of TRβV genes across the different conditions. c. Shannon entropy to estimate TRβV gene diversity. d. Plot comparing the mean expression levels of the Slow-Relaxing Module (SModule) for T cells from the indicated conditions grouped by TRβV genes.
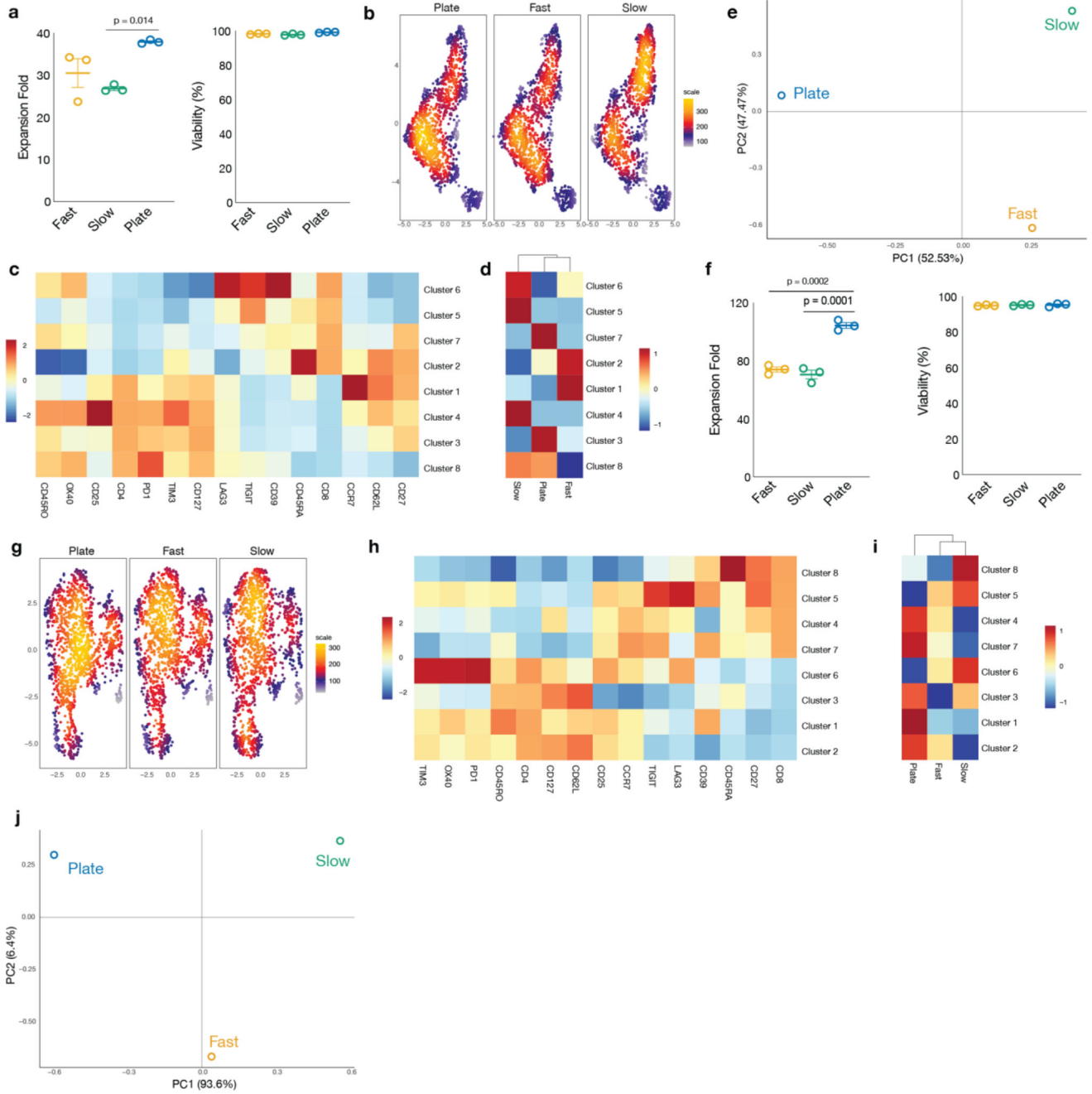
**Extended Fig. 9. T cell phenotypes persist after they are harvested from matrices.**
T cells were first cultured on plates or in fast relaxing or slow relaxing collagen
matrices, after which they were harvested and subsequently cultured in suspension with
or without dynabead restimulation. a-e. T cell phenotyping without dynabead restimulation.
a. Expansion fold (left) and viability (right) of T cells cultured in suspension after they
were harvested from their indicated matrices. b. Umap plots of phenotyped T cells. c-d.
K-means clustering was performed on pooled T cells from all experimental conditions. c.
Heatmap plot showing characteristic markers for each cluster. d. Heatmap plot showing the

frequencies of cells per condition for each cluster. e. PCA plot showing relative similarities between the different conditions. Data for b-d show pooled samples for n=3 replicates. f-j. Similar analyses as a-e but for T cells cultured with dynabead restimulation.
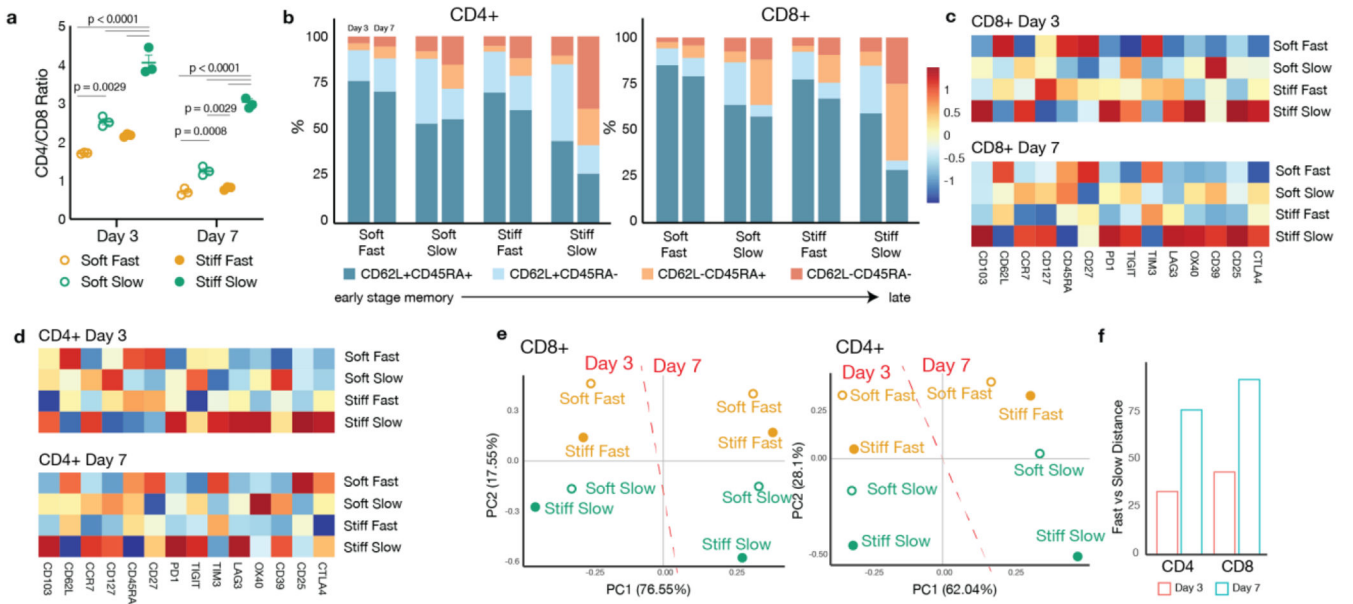


**Extended Fig. 10. Extended profiling and long-term imprinting of T cell Phenotype.**
a. CD4/CD8 ratios of T cells cultured in fast relaxing and slow relaxing, soft and stiff collagen gels for 3 days and 7 days. P-values were determined by performing two-tailed one-way Anova with Tukey post-hoc test. Data shows n=3 samples. b. CD62L and CD45RA expression profiles for CD4+ and CD8+ T cells cultured in different collagen conditions for 3 days and 7 days. c-d. Heatmaps for CD8+ T cells (c) and CD4+ T cells (d) showing relative marker expression levels between the different gel conditions. e. PCA plots showing relative similarities between the different collagen conditions for CD4+ and CD8+ T cells. f. Imprinting of T cell phenotype: T cells were harvested from collagen gels after 3-day and 7-day gel culture and further cultured in suspension for 7 days. The plot shows pairwise distances between T cells harvested from fast relaxing and slow relaxing collagen gels after suspension culture, showing greater differences between T cells cultured in collagen gels for 7 days. Data shows pooled samples n=3.
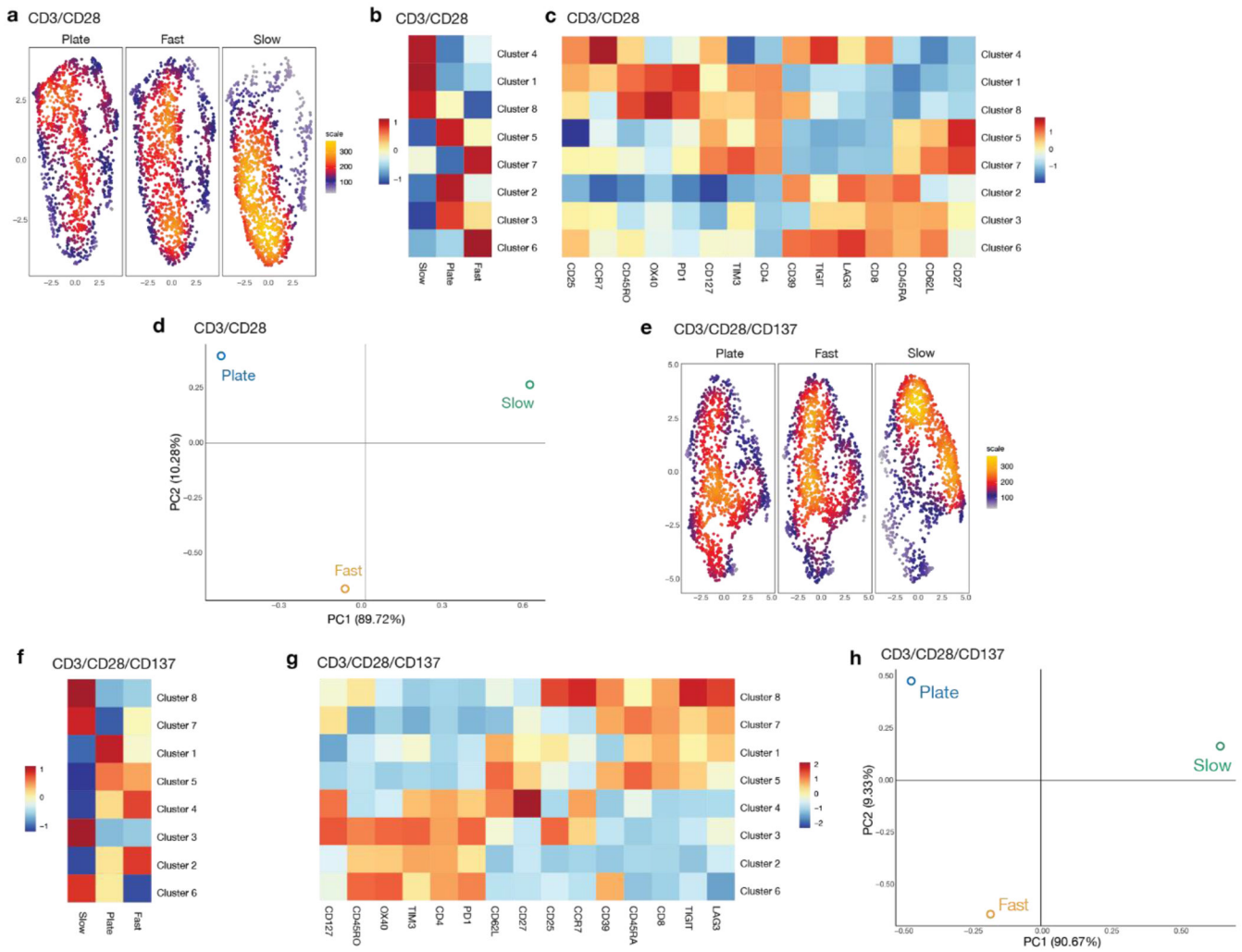
**Extended Fig. 11. ECM viscoelasticity modulates the phenotypes of T cells subjected to different modes of prior activation.**

a. Umap plots of phenotyped T cells after stimulation with aCD3/aCD28 dynabeads. b-c. K-means clustering was performed on pooled T cells from all experimental conditions. b. Heatmap plot showing the frequencies of cells per condition for each cluster. c. Heatmap plot showing characteristic markers for each cluster. d. PCA plot showing relative similarities between the different conditions. Data for a-d show pooled samples for n=3 replicates. e-h. Similar analyses as a-d but for T cells stimulated with aCD3/aCD28/aCD137 dynabeads.
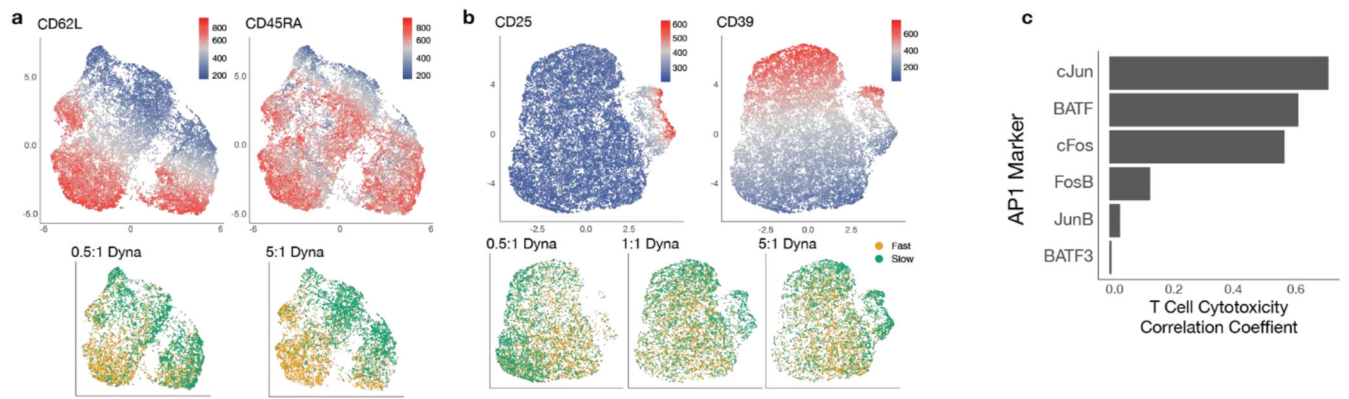
**Extended Fig. 12. Characterizing T cell phenotype and AP-1 correlation with T cell cytotoxicity.**
a. Representative umap plots of CD8+ T cells showing expression of CD62L (left) and
CD45RA (right), as well as localization of T cells (bottom) cultured in either fast relaxing
or slow relaxing gels, after T cells are activated with different dynabead to T cell ratios.
b. Representative umap plots showing expression of CD25 (left), CD39 (right) and T cell
localization (bottom) of the same collagen conditions used in a. Data shows pooled samples
n=3. c Correlation analyses showing how the expression of indicated AP-1 proteins for T
cells cultured in the different mechanical conditions correlate with their observed killing of
Raji cells.
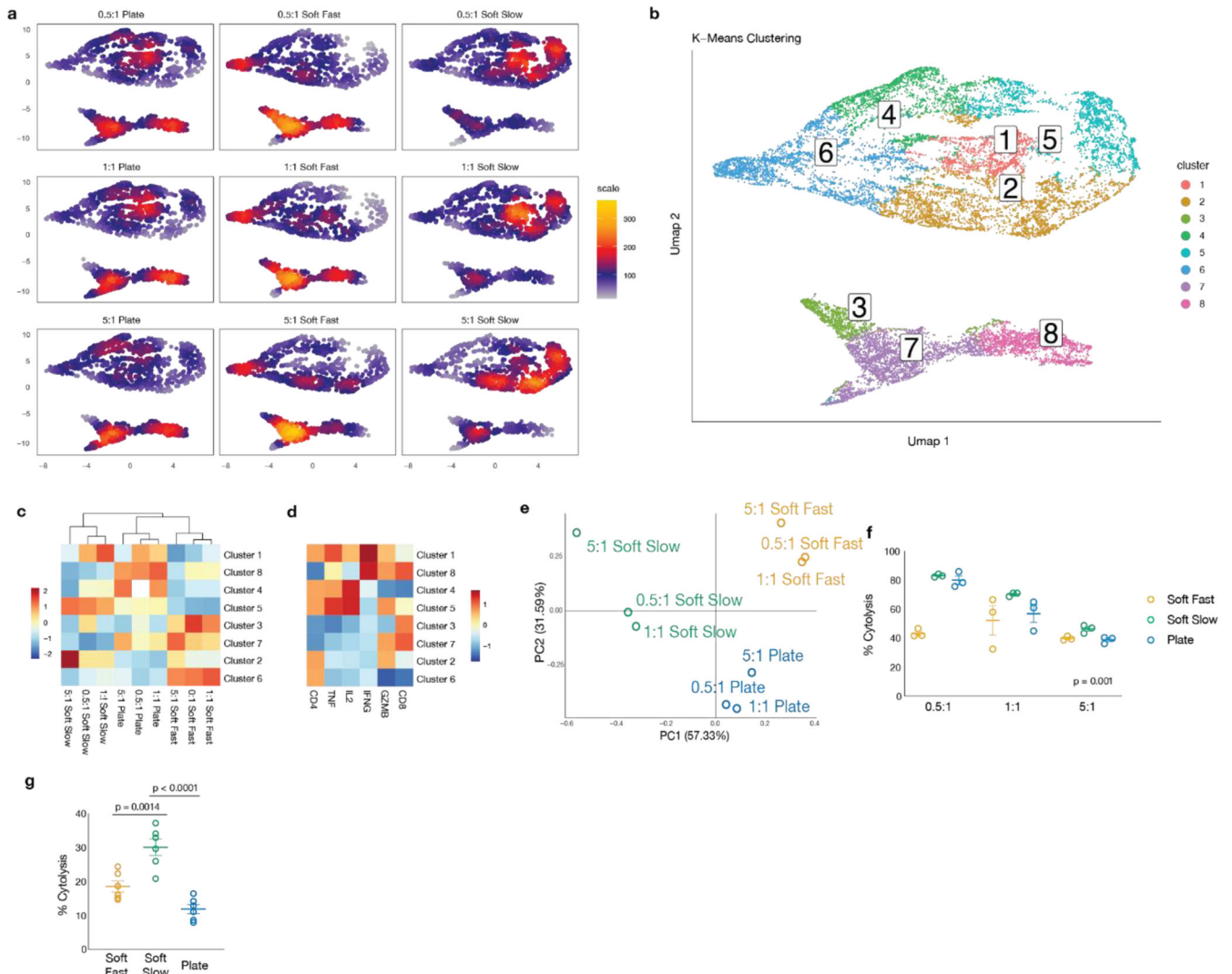
**Extended Fig. 13. T cells from different matrix conditions are functionally distinct against different tumor types.**

a-e. Human anti-CD19 CAR T cells were first activated using different dynabead to T cell ratios, subsequently cultured in fast relaxing, slow relaxing matrices or plate-culture and then co-cultured with Raji tumor cells. a. Umap plots of anti-CD19 CAR T cells phenotyped for their intracellular cytokine profiles after co-culture with Raji tumor cells. b-d. K-means clustering was performed on pooled T cells from all experimental conditions b. Umap plot of T cells overlaid with corresponding K-means clusters. c. Heatmap plot showing characteristic markers for each cluster. d. Heatmap plot showing the frequencies of cells per condition for each cluster. e. PCA plot showing relative similarities between the different conditions. Data shows pooled samples n=3. f. Differential levels of anti-CD19 CAR T cell killing of Raji cells after plate-culture or culturing in different matrix conditions. P-values were calculated by using two-way Anova for n=3 samples per dynabead stimulation level. g. Mouse Pmel-1 T cells were cultured in fast relaxing, slow relaxing matrices or plate-culture and subsequently co-cultured with B16-F10 melanoma cells. Plot shows differential killing

of B16-F10 tumor cells by Pmel-1 T cells. P-values were determined by performing two-tailed one-way ANOVA for n=6, 2 independent experiments.
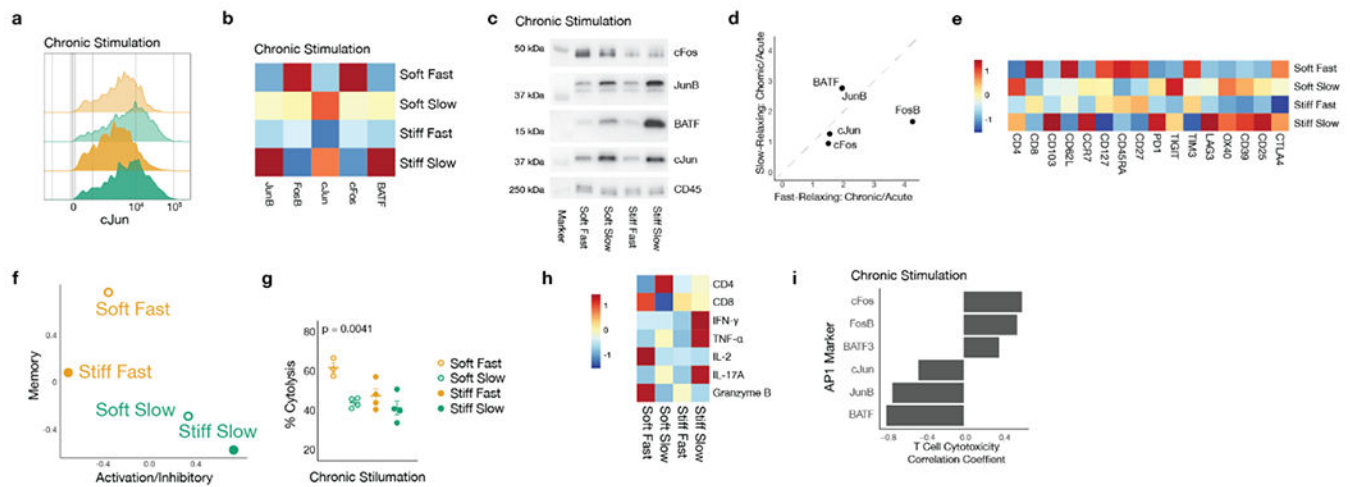


**Extended Fig. 14. ECM viscoelasticity modulates the phenotype and function of T cells undergoing chronic stimulation.**

a-d. Determination of AP-1 protein expression and interactions after chronic stimulation in matrices. a. Representative flow cytometry histograms showing relative expression of c-Jun for T cells cultured in fast relaxing and slow relaxing, soft and stiff matrices after chronic stimulation. b. Heatmap plot showing relative expression of indicated AP-1 proteins for T cells cultured in the different collagen conditions after chronic stimulation. c. c-Jun co-immunoprecipitation was performed to probe for c-Jun binding partners. Western blots compare relative amounts of indicated proteins bound to c-Jun as a function of the different mechanical conditions. d. Comparison of the extent to which the individual AP-1 proteins changed between T cells with and without chronic stimulation for the different gel conditions. Data shows pooled samples n=2-4. e-f. T cell phenotyping after chronic stimulation in collagen matrices. e. Heatmap plot comparing marker expression for the different collagen conditions. f. Plot showing memory and activation/inhibitory signatures for T cells cultured in the different gel conditions receiving chronic stimulation. Data shows pooled samples n=2-4. g. Differential levels of anti-CD19 CAR T cell killing of Raji cells after chronic stimulation in collagen matrices. P-values were calculated by using two-tailed one-way Anova for n=3-4 samples. h. Heatmap plot showing production of different cytokines and effector molecules by chronically stimulated anti-CD19 CAR T cells after co-culture with Raji cells. i. Correlation analyses showing how the expression of indicated AP-1 proteins for T cells cultured in the different mechanical conditions correlate with their observed killing of Raji cells after chronic stimulation.
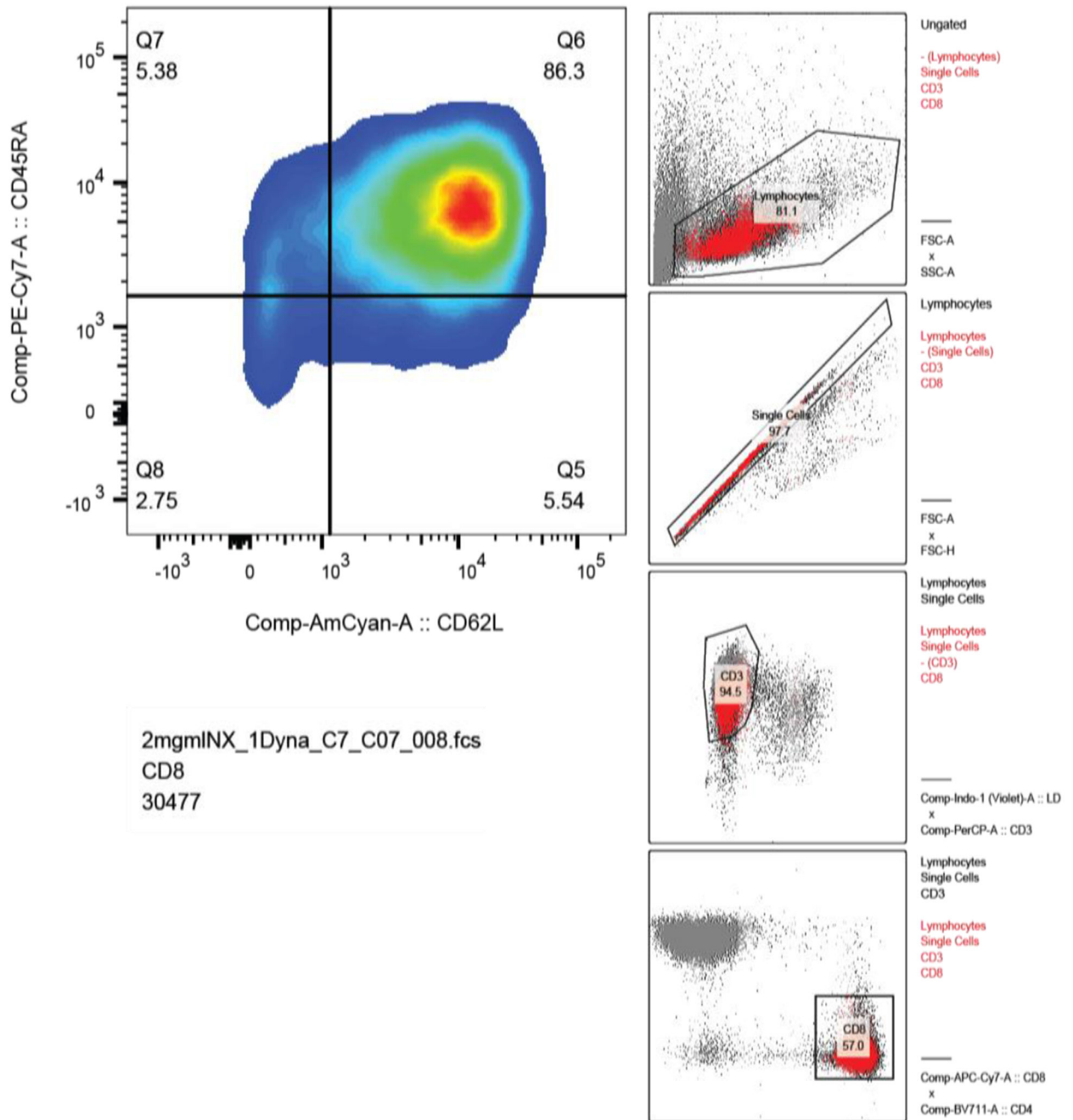
**Extended Fig. 15. Flow cytometry gating strategy.**

Representative flow cytometry gating strategy showing steps from ungated population to CD62L and CD4RA populations.

## Supplementary Material

Refer to Web version on PubMed Central for supplementary material.

## Acknowledgements

## Data Availability

Single cell rna-seq data will be deposited to NCBI GEO and made available after revision of this manuscript. Requests for all other raw or analyzed data will be made available upon request. The following RNA-Sequencing datasets used to validate our in vitro findings were assessed from publicly available GEO repository: NSCLC (GSE99254), Liver Cancer (GSE98638), Colorectal Cancer (GSE108989), Breast Cancer (GSE114727), Liver Fibrosis (GSE136103), IPF (GSE135893, GSE159354), Bulk RNA sequencing dataset (GSE126117).

## References

1. Reddy ST The patterns of T-cell target recognition. Nature 547, 36–38 (2017). [PubMed: 28636588]

2. Chaplin DD Overview of the Immune Response. J Allergy Clin Immunol 125, S3–23 (2010). [PubMed: 20176265]

3. Adu-Berchie K & Mooney DJ Biomaterials as Local Niches for Immunomodulation. Acc. Chem. Res. 53, 1749–1760 (2020). [PubMed: 32786230]

4. Met Ö, Jensen KM, Chamberlain CA, Donia M & Svane IM Principles of adoptive T cell therapy in cancer. Semin Immunopathol 41, 49–58 (2019). [PubMed: 30187086]

5. June CH, Riddell SR & Schumacher TN Adoptive cellular therapy: A race to the finish line. Science Translational Medicine 7, 280ps7–280ps7 (2015).

6. Pampusch MS et al. Rapid Transduction and Expansion of Transduced T Cells with Maintenance of Central Memory Populations. Molecular Therapy - Methods & Clinical Development 16, 1–10 (2020). [PubMed: 31673565]

7. Kalos M et al. T Cells with Chimeric Antigen Receptors Have Potent Antitumor Effects and Can Establish Memory in Patients with Advanced Leukemia. Sci Transl Med 3, 95ra73 (2011).

8. Redeker A & Arens R Improving Adoptive T Cell Therapy: The Particular Role of T Cell Costimulation, Cytokines, and Post-Transfer Vaccination. Frontiers in Immunology 7, 345 (2016). [PubMed: 27656185]

9. Global Manufacturing of CAR T Cell Therapy. Molecular Therapy - Methods & Clinical Development 4, 92–101 (2017). [PubMed: 28344995]

10. Hunder NN et al. Treatment of Metastatic Melanoma with Autologous CD4+ T Cells against NY-ESO-1. http://dx.doi.org/10.1056/NEJMoa0800251 https://www.nejm.org/doi/10.1056/NEJMoa0800251?url_ver=Z39.88-2003&rfr_id=ori%3Arid%3Acrossref.org&rfr_dat=cr_pub%3Dwww.ncbi.nlm.nih.gov (2009) doi:10.1056/NEJMoa0800251.

11. Cheung AS, Zhang DKY, Koshy ST & Mooney DJ Scaffolds that mimic antigen-presenting cells enable ex vivo expansion of primary T cells. Nature Biotechnology 36, 160–169 (2018).

12. McGarrity GJ et al. Patient monitoring and follow-up in lentiviral clinical trials. The Journal of Gene Medicine 15, 78–82 (2013). [PubMed: 23322669]

13. Huls MH et al. Clinical Application of Sleeping Beauty and Artificial Antigen Presenting Cells to Genetically Modify T Cells from Peripheral and Umbilical Cord Blood. J Vis Exp 50070 (2013) doi:10.3791/50070.

14. Beatty GL et al. Mesothelin-specific Chimeric Antigen Receptor mRNA-Engineered T cells Induce Anti-Tumor Activity in Solid Malignancies. Cancer Immunol Res 2, 112–120 (2014). [PubMed: 24579088]

15. Gett AV, Sallusto F, Lanzavecchia A & Geginat J T cell fitness determined by signal strength. Nat Immunol 4, 355–360 (2003). [PubMed: 12640450]

16. Masopust D, Vezys V, Wherry EJ, Barber DL & Ahmed R Cutting Edge: Gut Microenvironment Promotes Differentiation of a Unique Memory CD8 T Cell Population. The Journal of Immunology 176, 2079–2083 (2006). [PubMed: 16455963]

17. Schenkel JM & Masopust D Tissue-Resident Memory T Cells. Immunity 41, 886–897 (2014). [PubMed: 25526304]

18. Szabo PA et al. Single-cell transcriptomics of human T cells reveals tissue and activation signatures in health and disease. Nature Communications 10, 1–16 (2019).

19. Wells RG Tissue Mechanics and Fibrosis. Biochim Biophys Acta 1832, 884–890 (2013). [PubMed: 23434892]

20. Chaudhuri O, Cooper-White J, Janmey PA, Mooney DJ & Shenoy VB Effects of extracellular matrix viscoelasticity on cellular behaviour. Nature 584, 535–546 (2020). [PubMed: 32848221]

21. Boraschi-Diaz I, Wang J, Mort JS & Komarova SV Collagen Type I as a Ligand for Receptor-Mediated Signaling. Frontiers in Physics 5, 12 (2017).

22. Guo X et al. Global characterization of T cells in non-small-cell lung cancer by single-cell sequencing. Nat Med 24, 978–985 (2018). [PubMed: 29942094]

23. Zheng C et al. Landscape of Infiltrating T Cells in Liver Cancer Revealed by Single-Cell Sequencing. Cell 169, 1342–1356.e16 (2017). [PubMed: 28622514]

24. Zhang L et al. Lineage tracking reveals dynamic relationships of T cells in colorectal cancer. Nature 564, 268–272 (2018). [PubMed: 30479382]

25. Secomb TW & Pries AR Blood viscosity in microvessels: experiment and theory. C R Phys 14, 470–478 (2013). [PubMed: 25089124]

26. Liu C, Pei H & Tan F Matrix Stiffness and Colorectal Cancer. Onco Targets Ther 13, 2747–2755 (2020). [PubMed: 32280247]

27. Huang J et al. Extracellular matrix and its therapeutic potential for cancer treatment. Sig Transduct Target Ther 6, 1–24 (2021).

28. L. Oliveira B, Guo Z & L. Bernardes GJ Inverse electron demand Diels–Alder reactions in chemical biology. Chemical Society Reviews 46, 4895–4950 (2017). [PubMed: 28660957]

29. Vining KH & Mooney DJ Mechanical forces direct stem cell behaviour in development and regeneration. Nat Rev Mol Cell Biol 18, 728–742 (2017). [PubMed: 29115301]

30. Butcher DT, Alliston T & Weaver VM A tense situation: forcing tumour progression. Nat Rev Cancer 9, 108–122 (2009). [PubMed: 19165226]

31. Levental KR et al. Matrix Crosslinking Forces Tumor Progression by Enhancing Integrin signaling. Cell 139, 891–906 (2009). [PubMed: 19931152]

32. Kass L, Erler JT, Dembo M & Weaver VM Mammary epithelial cell: Influence of extracellular matrix composition and organization during development and tumorigenesis. The International Journal of Biochemistry & Cell Biology 39, 1987–1994 (2007). [PubMed: 17719831]

33. Cox TR & Erler JT Remodeling and homeostasis of the extracellular matrix: implications for fibrotic diseases and cancer. Dis Model Mech 4, 165–178 (2011). [PubMed: 21324931]

34. Staunton JR et al. Mechanical properties of the tumor stromal microenvironment probed in vitro and ex vivo by in situ-calibrated optical trap-based active microrheology. Cell Mol Bioeng 9, 398–417 (2016). [PubMed: 27752289]

35. Kotliar D et al. Identifying gene expression programs of cell-type identity and cellular activity with single-cell RNA-Seq. eLife 8, e43803 (2019). [PubMed: 31282856]

36. Bediaga NG et al. Multi-level remodelling of chromatin underlying activation of human T cells. Sci Rep 11, 528 (2021). [PubMed: 33436846]

37. Azizi E et al. Single-Cell Map of Diverse Immune Phenotypes in the Breast Tumor Microenvironment. Cell 174, 1293–1308.e36 (2018). [PubMed: 29961579]

38. Weiskirchen R, Weiskirchen S & Tacke F Organ and tissue fibrosis: Molecular signals, cellular mechanisms and translational implications. Molecular Aspects of Medicine 65, 2–15 (2019). [PubMed: 29958900]

39. Dobie R et al. Single-Cell Transcriptomics Uncovers Zonation of Function in the Mesenchyme during Liver Fibrosis. Cell Reports 29, 1832–1847.e8 (2019). [PubMed: 31722201]

40. Single-cell RNA sequencing reveals profibrotic roles of distinct epithelial and mesenchymal lineages in pulmonary fibrosis. 10.1126/sciadv.aba1972.

41. DePianto DJ et al. Molecular mapping of interstitial lung disease reveals a phenotypically distinct senescent basal epithelial cell population. JCI Insight 6, (2021).

42. Lynn RC et al. c-Jun overexpression in CAR T cells induces exhaustion resistance. Nature 576, 293–300 (2019). [PubMed: 31802004]

43. Kurachi M et al. The transcription factor BATF operates as an essential differentiation checkpoint in early effector CD8+ T cells. Nat Immunol 15, 373–383 (2014). [PubMed: 24584090]

44. Quigley M et al. Transcriptional analysis of HIV-specific CD8+ T cells shows that PD-1 inhibits T cell function by upregulating BATF. Nat Med 16, 1147–1151 (2010). [PubMed: 20890291]

45. Seo H et al. BATF and IRF4 cooperate to counter exhaustion in tumor-infiltrating CAR T cells. Nat Immunol 22, 983–995 (2021). [PubMed: 34282330]

46. Koizumi S et al. JunB regulates homeostasis and suppressive functions of effector regulatory T cells. Nat Commun 9, 5344 (2018). [PubMed: 30559442]

47. jun-B inhibits and c-fos stimulates the transforming and trans-activating activities of c-jun - ScienceDirect. https://www.sciencedirect.com/science/article/pii/0092867489907551?via%3Dihub.

48. Chiu R, Angel P & Karin M Jun-B differs in its biological properties from, and is a negative regulator of, c-Jun. Cell 59, 979–986 (1989). [PubMed: 2513128]

49. Atsaves V, Leventaki V, Rassidakis GZ & Claret FX AP-1 Transcription Factors as Regulators of Immune Responses in Cancer. Cancers (Basel) 11, 1037 (2019). [PubMed: 31340499]

50. Bennett BL et al. SP600125, an anthrapyrazolone inhibitor of Jun N-terminal kinase. Proceedings of the National Academy of Sciences 98, 13681–13686 (2001).

51. Kullmann A et al. CD137 for Isolation and Expansion of Ag-specific T cells using Dynabeads®. 1.

52. Ji Y et al. Identification of the Genomic Insertion Site of Pmel-1 TCR α and β Transgenes by Next-Generation Sequencing. PLOS ONE 9, e96650 (2014). [PubMed: 24827921]

53. Overwijk WW et al. Tumor Regression and Autoimmunity after Reversal of a Functionally Tolerant State of Self-reactive CD8+ T Cells. Journal of Experimental Medicine 198, 569–580 (2003). [PubMed: 12925674]

54. T Cell TransActTM, human | Polyclonal stimulation | Stimulation reagents | MACS Cell Culture and Stimulation | Products | Miltenyi Biotec | USA. https://www.miltenyibiotec.com/US-en/products/t-cell-transact-human.html#130-111-160.

55. Meng KP, Majedi FS, Thauland TJ & Butte MJ Mechanosensing through YAP controls T cell activation and metabolism. Journal of Experimental Medicine 217, (2020).

56. Judokusumo E, Tabdanov E, Kumari S, Dustin ML & Kam LC Mechanosensing in T Lymphocyte Activation. Biophysical Journal 102, L5–L7 (2012). [PubMed: 22339876]

57. O'Connor RS et al. Substrate Rigidity Regulates Human T Cell Activation and Proliferation. The Journal of Immunology 189, 1330–1339 (2012). [PubMed: 22732590]

58. Liu B, Chen W, Evavold BD & Zhu C Accumulation of Dynamic Catch Bonds between TCR and Agonist Peptide-MHC Triggers T Cell Signaling. Cell 157, 357–368 (2014). [PubMed: 24725404]

59. Kim ST et al. TCR Mechanobiology: Torques and Tunable Structures Linked to Early T Cell Signaling. Front. Immunol 3, (2012).

60. Wang J-H T cell receptors, mechanosensors, catch bonds and immunotherapy. Prog Biophys Mol Biol 153, 23–27 (2020). [PubMed: 32006526]

61. Das DK et al. Force-dependent transition in the T-cell receptor β-subunit allosterically regulates peptide discrimination and pMHC bond lifetime. PNAS 112, 1517–1522 (2015). [PubMed: 25605925]

62. Lambert LH et al. Improving T Cell Expansion with a Soft Touch. Nano Lett. 17, 821–826 (2017). [PubMed: 28122453]

63. Hickey JW et al. Engineering an Artificial T-Cell Stimulating Matrix for Immunotherapy. Adv Mater 31, e1807359 (2019). [PubMed: 30968468]

64. Majedi FS et al. T-cell activation is modulated by the 3D mechanical microenvironment. Biomaterials 252, 120058 (2020). [PubMed: 32413594]

65. Kuczek DE et al. Collagen density regulates the activity of tumor-infiltrating T cells. Journal for ImmunoTherapy of Cancer 7, 68 (2019). [PubMed: 30867051]

66. Park SL, Gebhardt T & Mackay LK Tissue-Resident Memory T Cells in Cancer Immunosurveillance. Trends in Immunology 40, 735–747 (2019). [PubMed: 31255505]

67. Beura LK et al. Intravital mucosal imaging of CD8+ resident memory T cells shows tissue-autonomous recall responses that amplify secondary memory. Nat Immunol 19, 173–182 (2018). [PubMed: 29311694]

68. Wernig G et al. Unifying mechanism for different fibrotic diseases. PNAS 114, 4757–4762 (2017). [PubMed: 28424250]

69. Cui L et al. Activation of JUN in fibroblasts promotes pro-fibrotic programme and modulates protective immunity. Nat Commun 11, 2795 (2020). [PubMed: 32493933]

70. Schulien I et al. The transcription factor c-Jun/AP-1 promotes liver fibrosis during non-alcoholic steatohepatitis by regulating Osteopontin expression. Cell Death Differ 26, 1688–1699 (2019). [PubMed: 30778201]

71. Transcription Factor IRF4 Promotes CD8+ T Cell Exhaustion and Limits the Development of Memory-like T Cells during Chronic Infection - ScienceDirect. https://www-sciencedirect-com.ezp-prod1.hul.harvard.edu/science/article/pii/S1074761317305228?via%3Dihub.

72. Papavassiliou AG & Musti AM The Multifaceted Output of c-Jun Biological Activity: Focus at the Junction of CD8 T Cell Activation and Exhaustion. Cells 9, 2470 (2020). [PubMed: 33202877]

Author Manuscript

Author Manuscript

Author Manuscript

Author Manuscript
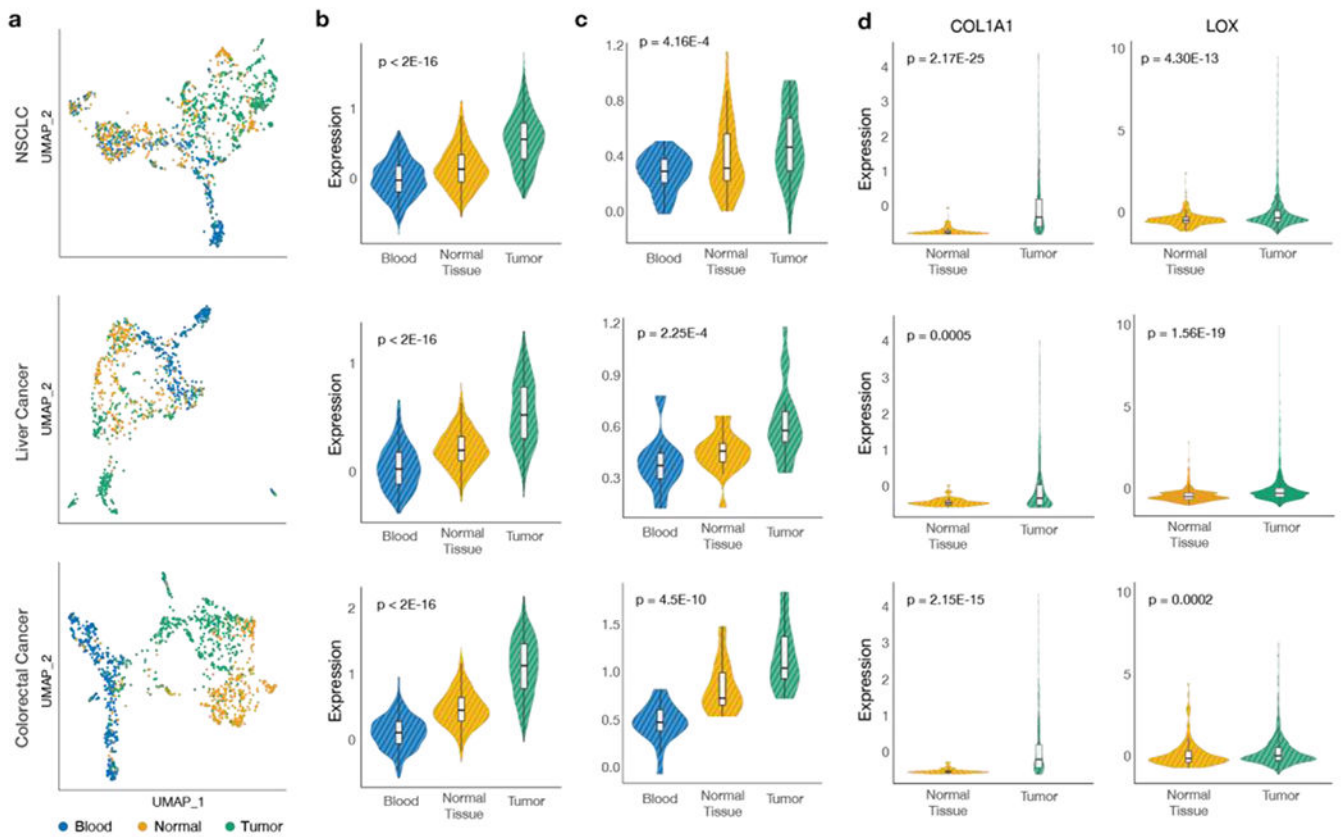
**Fig. 1. Tissue microenvironment influences T cell phenotype.**

a. Umap plots of pan CD8+ T cells from tumors, adjacent normal tissue and blood for NSCLC, liver cancer, and colorectal cancer. b-c. Violin plots comparing expression levels of tumor T cell gene signatures for T cells located in tumors, normal tissues and blood for (b) pan T cells or (c) T cells with shared TCR clonotypes. P-values were determined by performing two-tailed one-way Anova. d. Relative expression of collagen type I (COL1A1) and lysyl oxidase (LOX) in normal tissues and tumors from the TCGA dataset. P-values were determined by performing Wilcoxon signed-rank test.
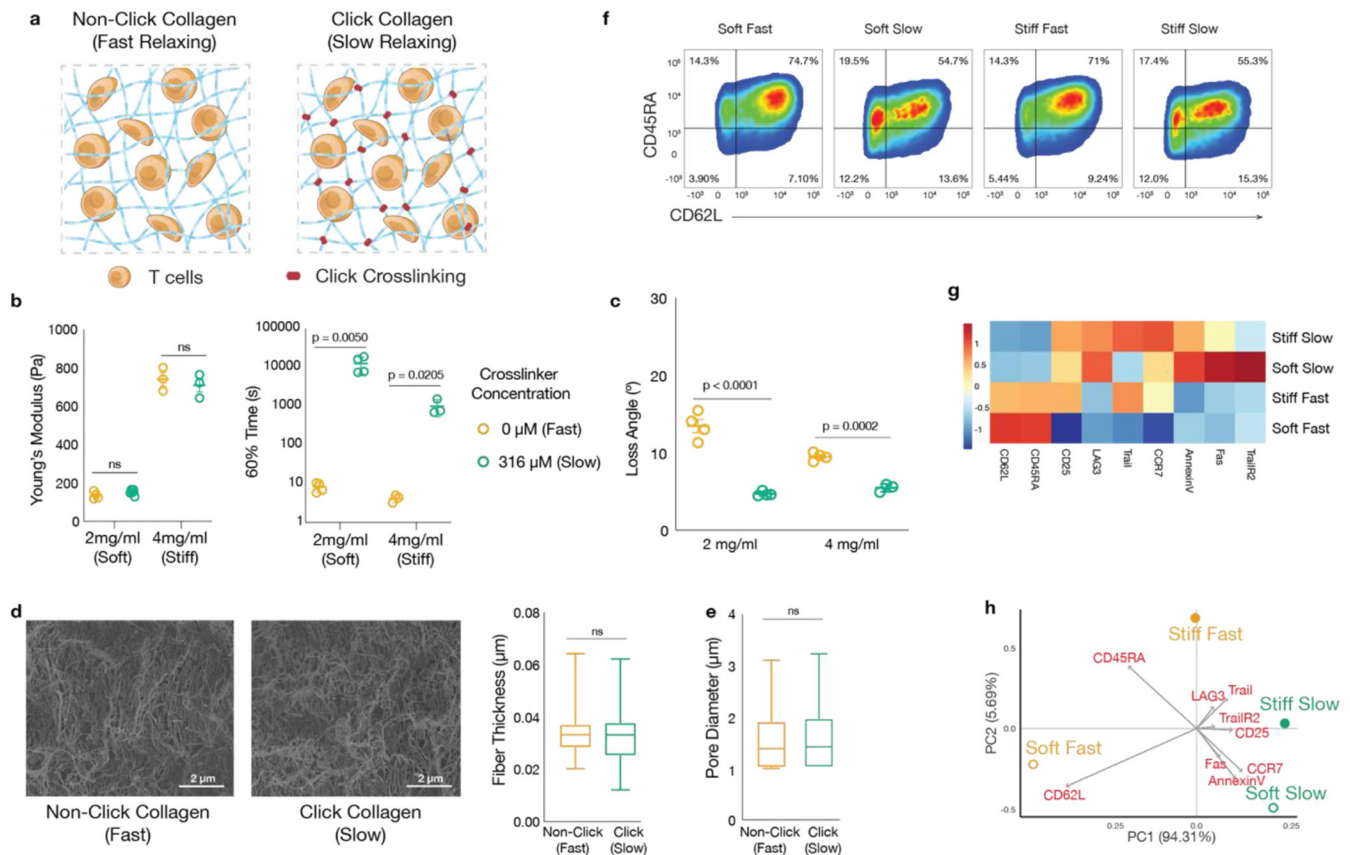
**Fig. 2. Synthesizing collagen-based ECM mimetic with tunable mechanical properties.**
a. Schematic of collagen type I based ECM mimetic showing non-click collagen (fast relaxing) and click collagen (slow relaxing) matrices. b. Shear Young's moduli (left) and time values for relaxation to 60% of initial stress under constant deformation (right) for 2 mg/ml (soft) and 4 mg/ml (stiff) collagen matrices. P-values were determined by performing two-tailed unpaired t-test. Data are mean ± s.e.m from n=3-5. Significance threshold: $P<0.05$ (ns=not significant). c. Loss angle measurements for collagen matrices. P-values were calculated by using two-tailed unpaired t-test for n=3-4 samples. d. Cryo-SEM images, fiber thickness and, e. pore size estimation for 2mg/ml fast and slow relaxing matrices showing that collagen architecture is maintained. P-values were determined using two-tailed unpaired t-test. Significance threshold: $P<0.05$. f. Representative flow cytometry plots showing CD62L and CD45RA expression, and (g) relative expression levels of various markers, in CD8+ T cells cultured in slow or fast relaxing, soft or stiff collagen matrices. h. PCA plots showing that phenotypic differences are driven more by changes in collagen viscoelasticity than by stiffness. Data shows pooled samples for n=3.
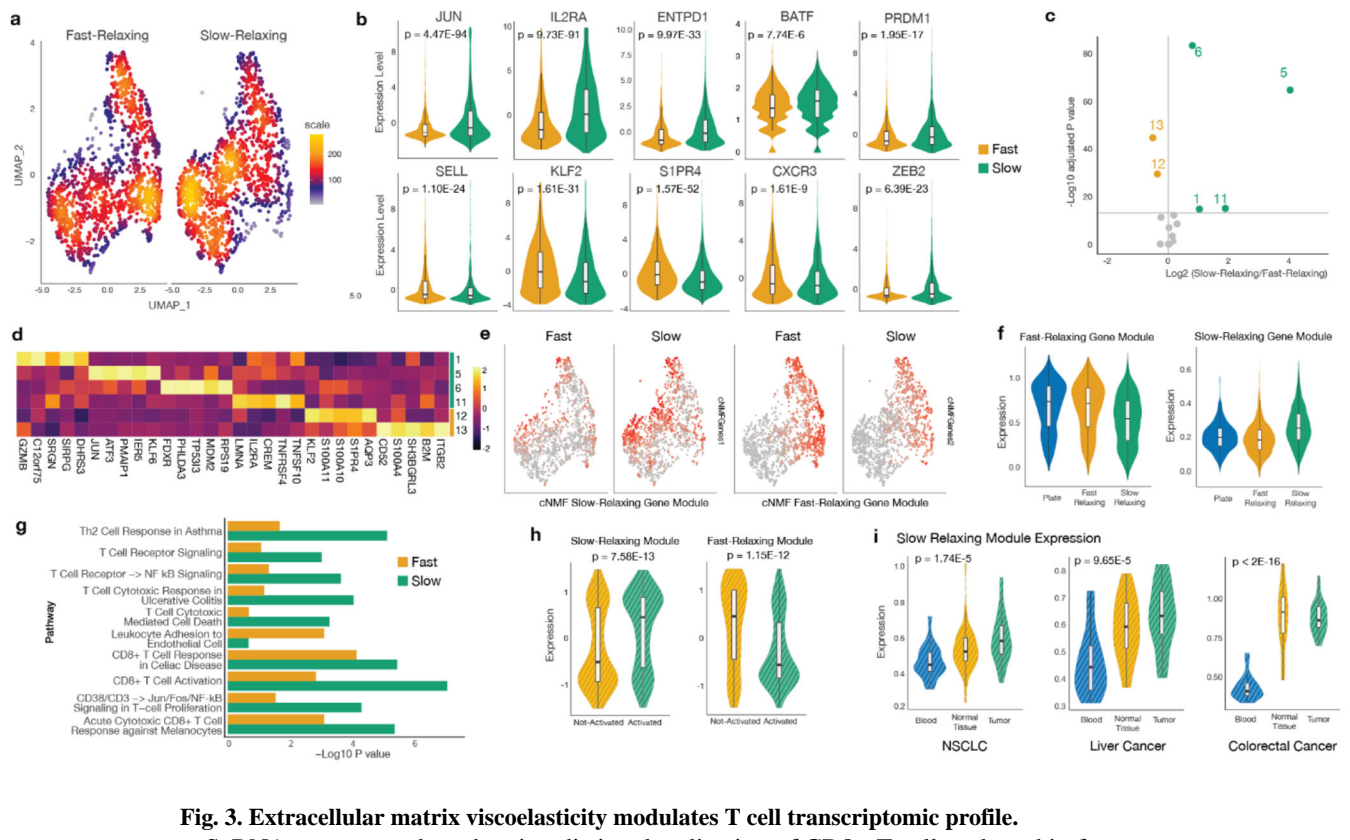
**Fig. 3. Extracellular matrix viscoelasticity modulates T cell transcriptomic profile.**
a. ScRNA-seq umap plots showing distinct localization of CD8+ T cells cultured in fast relaxing or slow relaxing collagen matrices. b. Violin plots comparing expression levels of selected genes. P-values were determined by performing differential gene expression in Seurat using a negative binomial generalized linear model. c. Volcano plot showing significant gene modules identified by consensus non-negative matrix factorization (cNMF) for T cells in fast relaxing (FModule, orange) and slow relaxing matrices (SModule, green). Module 5 is the most significantly enriched module in slow relaxing matrices. P-values were determined by performing Wilcoxon Rank Sum test adjusted with FDR. Significance threshold: −log10(Adjusted P-value)>15. d. Heatmap of representative genes that characterize FModule (12,13: orange) and SModule (1,2,4,11: green). Unique genes from the 4 SModule programs combined, as well as the 2 FModule programs. e. Umap overlay of aggregate expression levels of cNMF FModule and SModule showing distinct localizations that map to regions of high T cell density in fast relaxing and slow relaxing matrices respectively. f. Comparison of expression profiles of FModule and SModule between plate-cultured T cells (suspension culture; no collagen matrix condition), T cells in cultured in fast-relaxing and slow-relaxing collagen matrices. P-values were determined by performing two-tailed one-way Anova. g. Pathway analysis comparing enriched pathways for FModule and SModule, indicating a more activated T cell state in the SModule. h. Violin plots comparing expression levels of SModule and FModule in a published bulk RNA-seq dataset that profiled activated versus non-activated T cells, showing increased relative expression of SModule in activated T cells and vice versa. P-values were determined by performing Wilcoxon Rank Sum test adjusted with FDR. i. Violin plots comparing expression levels of SModule for T cells with shared TCR clonotypes in tumors, adjacent
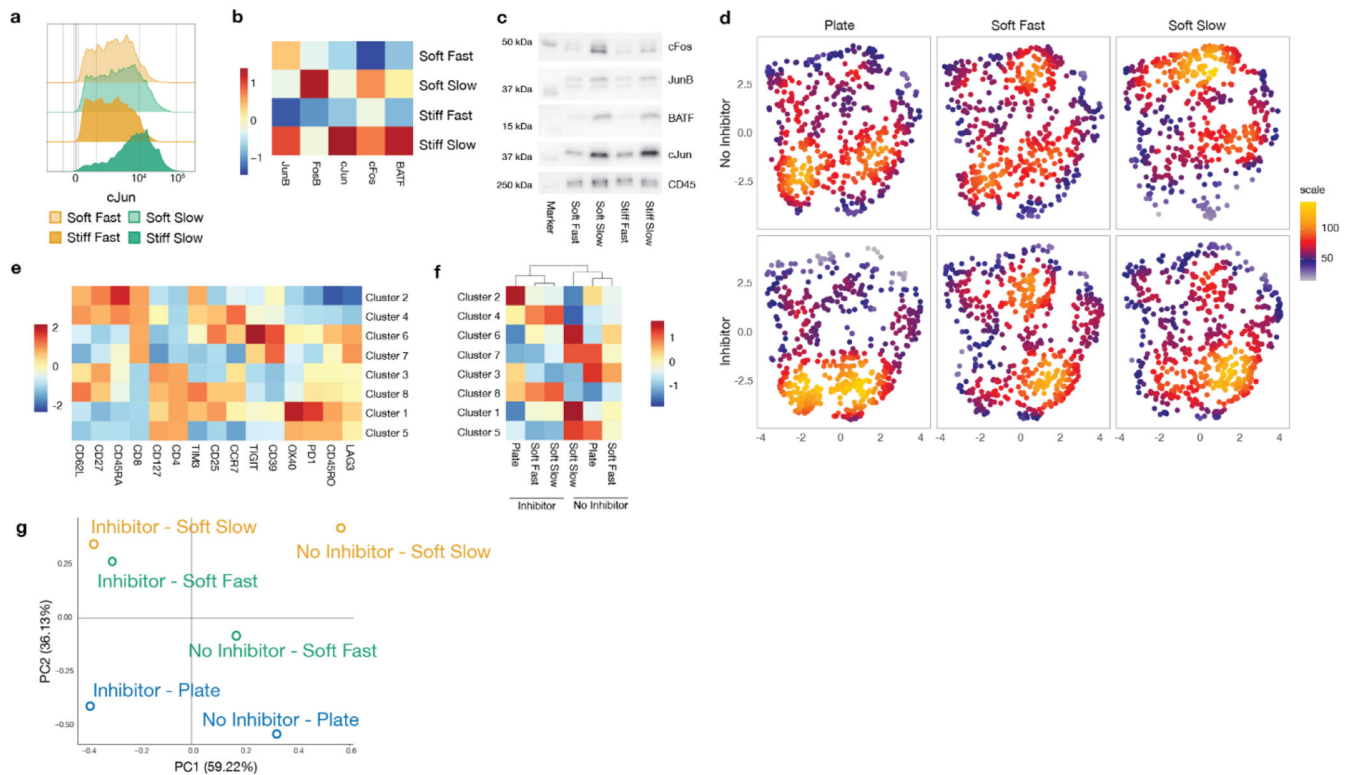
normal tissues and blood for NSCLC, liver cancer and colorectal cancer (same dataset used for Fig. 1a–c). P-values were determined by performing two-tailed one-way Anova.

**Fig. 4. T cell populations generated from ECM with different viscoelasticity have different patterns of AP-1 protein expression that can be abrogated by inhibitors.**
a. Representative flow cytometry histograms showing relative expression of c-Jun for T cells cultured in fast relaxing and slow relaxing, soft and stiff matrices after acute activation. b. Heatmap plot showing relative expression of indicated AP-1 proteins for T cells cultured in the different collagen conditions. c. c-Jun co-immunoprecipitation was performed to probe for c-Jun binding partners. Western blots compare relative amounts of indicated proteins bound to c-Jun as a function of the different mechanical conditions. Data shows pooled samples n=2-4. d. Umap plots of plate-cultured T cells and T cells cultured in fast or slow relaxing matrices with or without the SP600125 Jun N-terminal kinase inhibitor. e-g. K-means clustering was performed on pooled T cells from all experimental conditions. e. Heatmap plot showing characteristic markers for each cluster. f. Heatmap plot showing the frequencies of cells per condition for each cluster. g. PCA plot showing the relative similarities between the different conditions.
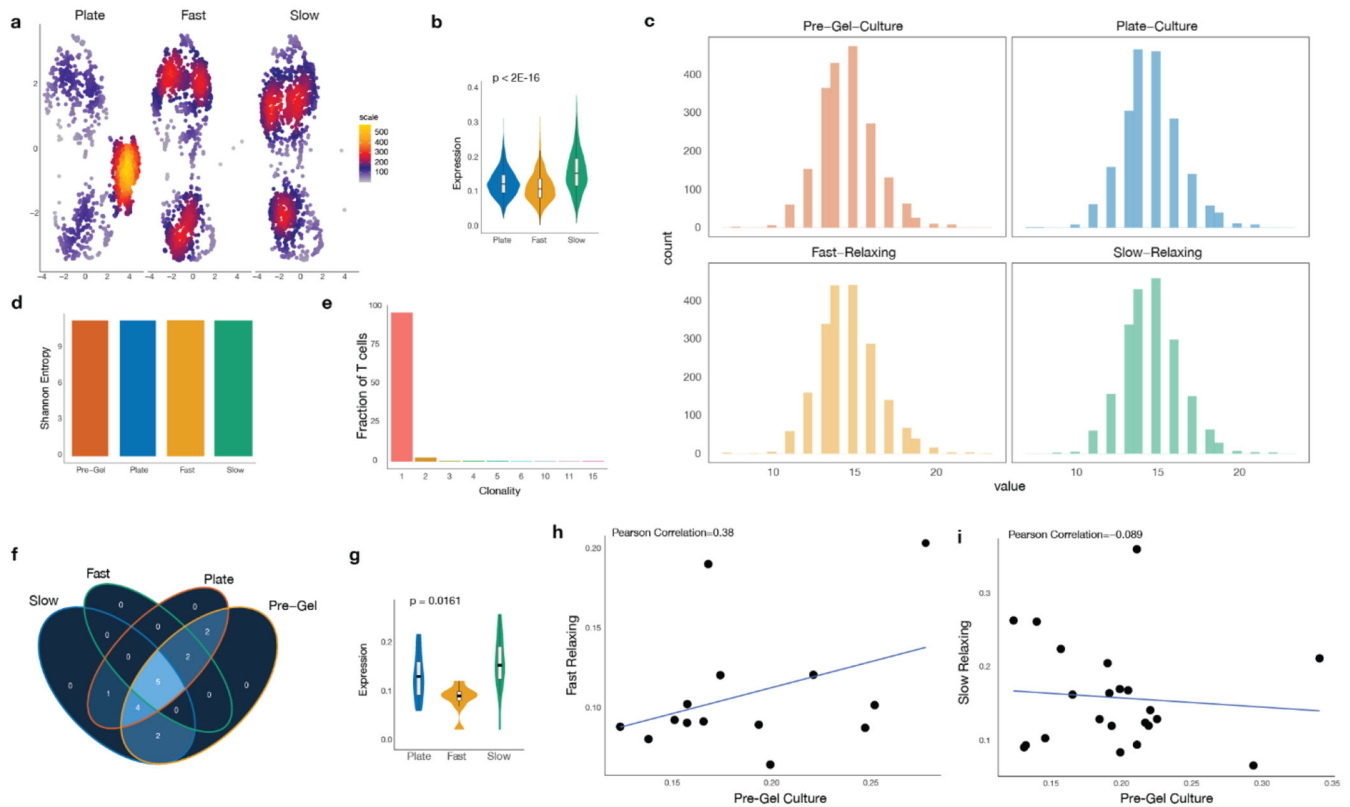
**Fig. 5. ECM viscoelasticity does not select for specific T cell clones.**
a. ScRNA-seq umap plots showing distinct localization of plate-cultured T cells, T cells cultured in fast relaxing or slow relaxing collagen matrices for a different donor. b. Violin plot comparing the expression levels of the Slow-Relaxing Module (SModule) generated in Fig. 3 for the different matrix conditions. P-values were determined by performing two-tailed one-way Anova. c. Histograms showing TCRβ CDR3 length distributions. Pre-Gel condition refers to the parent T cell population before they were embedded in the matrices. d. Shannon entropy plot comparing clonotypic diversity between the different conditions. e. Plot showing the proportions of combined T cells from all experimental conditions with unique TCRs and various degrees of clonality. f-g. Venn diagrams showing the distribution of dominant clones (f) across the different conditions. g. Violin plot comparing the expression levels of SModule for T cells with shared TCRs. P-values were determined by performing two-tailed one-way Anova. h-i. Pearson correlation plots for individual T cell clones before and after their culture in fast relaxing (i) or slow relaxing (j) collagen matrices.
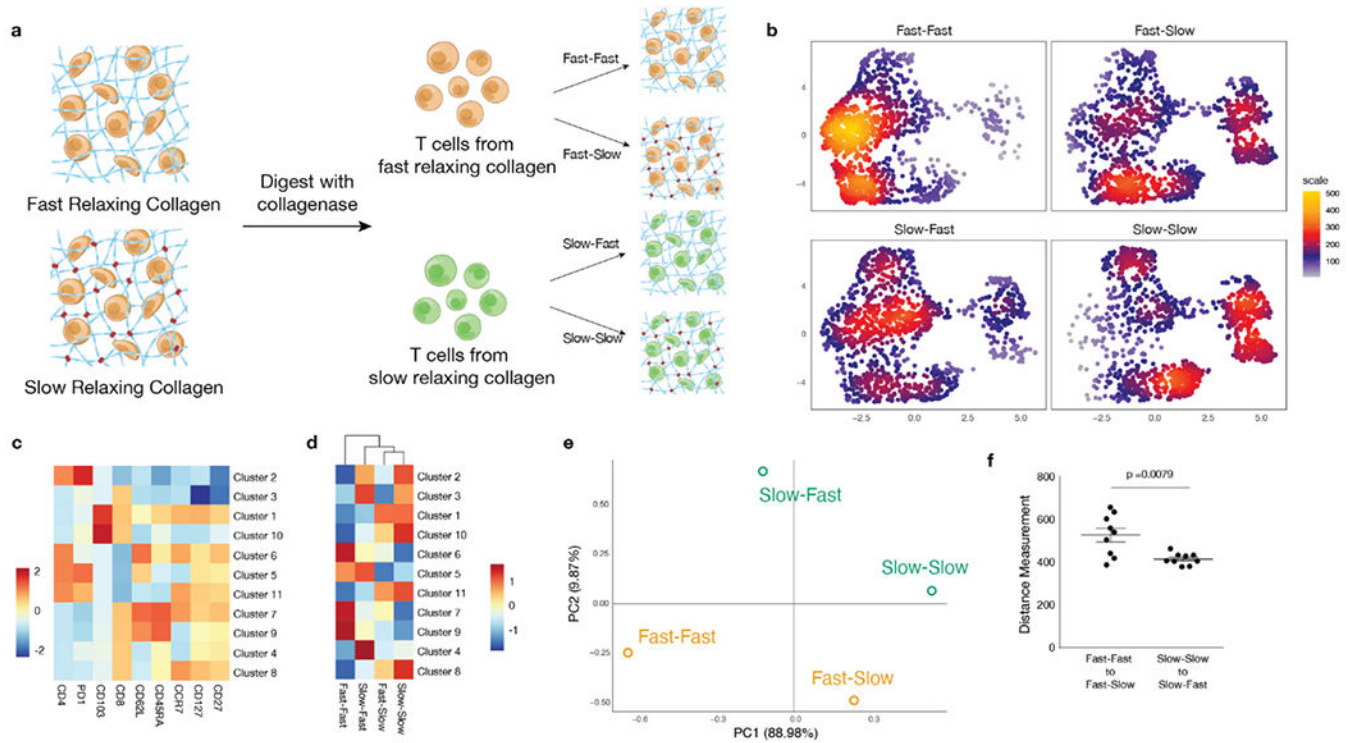
**Fig. 6. Prior matrix condition influences the phenotype of serially passaged T cells.**
a. Schematic of serial passaging experiment. T cells were either cultured in fast relaxing or slow relaxing matrices for 3 days, after which the cells were harvested and serially passaged as follows: fast relaxing to fast relaxing matrices (Fast-Fast), fast relaxing to slow relaxing matrices (Fast-Slow), slow relaxing to fast relaxing matrices (Slow-Fast) and slow relaxing to slow relaxing matrices (Slow-Slow) for an additional 4 days before analysis. b. Umap plots after performing flow cytometry on serially passaged T cells. c-d. K-means clustering was performed on pooled T cells from all experimental conditions. c. Heatmap plot showing characteristic markers for each cluster. d. Heatmap plot showing the frequencies of cells per condition for each cluster. e. PCA plot showing the relative similarities between the different conditions. f. Plot comparing the estimated Euclidean distances between the indicated conditions. P-values were determined by performing two-tailed unpaired t test with Welch's correction, with 9 pair-wise measurements from n=3 replicates.
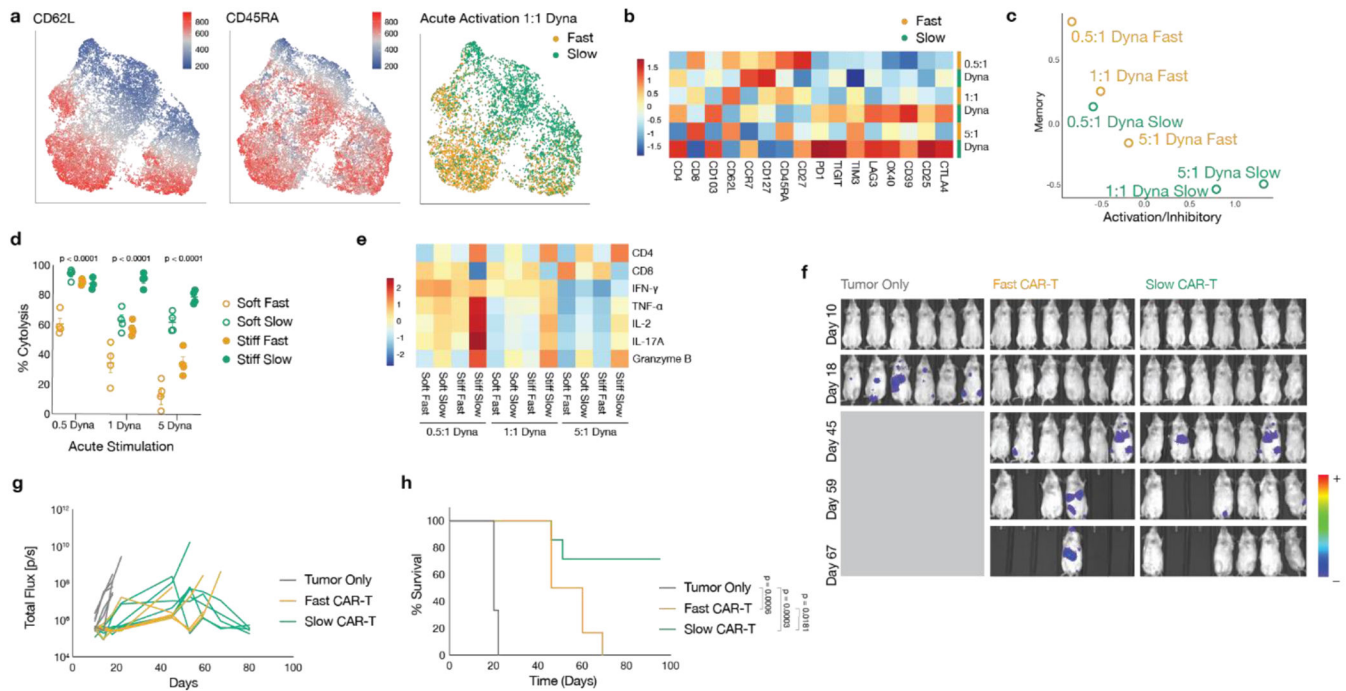
**Fig. 7. Tuning ECM viscoelasticity results in the generation of functionally distinct T cells.**
a-e, T cells were activated for 4 days using different dynabead to T cell ratios and subsequently cultured in fast relaxing or slow relaxing matrices. a. Representative umap plots of CD8+ T cells showing expression of CD62L (left) and CD45RA (center), as well as localization of T cells cultured in either fast relaxing or slow relaxing matrices (right). b. Heatmap plot showing relative marker expression as a function of fast relaxing (orange) and slow relaxing (green) matrices for the different dynabead to T cell ratios. c. Plot comparing memory (CD62L, CCR7, CD127, CD45RA, CD27) and activation/inhibitory (PD1, TIGIT, TIM3, LAG3, OX40, CD39, CD25, CTLA4) signatures for T cells cultured in fast relaxing and slow relaxing matrices. Data shows pooled samples n=3. d. Differential levels of anti-CD19 CAR T cell killing of Raji cells after culturing in different collagen conditions. P-values were calculated by using two-tailed one-way Anova for n=3-4 samples. e. Heatmap plot showing production of different cytokines and effector molecules by anti-CD19 CAR T cells after co-culture with Raji cells. f-h. Luciferized Raji xenograft lymphoma model. f-g. IVIS images (f) and total flux (g) of Raji tumor burden in NSG mice for the indicated conditions. h. Kaplan-Meier survival curves of mice from the indicated treatment groups. P-values were determined by Log-rank (Mantel-Cox) test. Data are n=6 or 7 mice per condition